NPL
National Physical Laboratory

NPL REPORT MAT 122

EFFECT OF SPECIMEN MISALIGNMENT IN STATIC AND FATIGUE TESTING OF SMALL-SCALE TEST PIECES

A T FRY, M J LODEIRO, A KOKO, F BOOTH-DOWNS, L E CROCKER

FEBRUARY 2023

EFFECT OF SPECIMEN MISALIGNMENT IN STATIC AND FATIGUE TESTING OF SMALL-SCALE TEST PIECES

A T FRY, M J LODEIRO, A KOKO, F BOOTH-DOWNS, L E CROCKER
Advanced Engineered Materials

ISSN 1754-2979

DOI: https://doi.org/10.47120/npl.MAT122

National Physical Laboratory
Hampton Road, Teddington, Middlesex, TW11 0LW

This work was funded by the UK Government's Department for Science, Innovation & Technology through the UK's National Measurement System programmes.

Approved on behalf of NPLML by
Stefanos Giannis, Science Area Leader, Advanced Engineered Materials.

CONTENTS

INTRODUCTION

Low cycle fatigue (LCF) tests simulating in-service conditions have long been known to be difficult to devise and perform. They can be expensive to execute and can frequently give unreliable results. They, however, remain essential for the safe design and operation of components occasionally stressed into the plastic region. In 1987 an intercomparison was conducted under the auspices of VAMAS, the Versailles Project on Advanced Materials and Standards. Technical Working Area (TWA) 13 was created and investigated the influence that specimen alignment played on LCF testing. Two studies were conducted within this exercise. The first objective of this study [1] generated LCF data at elevated temperature and aimed to identify aspects of the testing procedure that significantly affect the repeatability and reproducibility of the results. Analysis of the data generated concluded that the primary causes of inter-laboratory data variability were most likely associated with specimen bending due to misalignment in the test system's load-train, lateral rigidity of the test system, and errors in measuring and controlling the strain and the test temperature [2]. The second inter-laboratory study conducted aimed to produce a framework for quantifying the measurement uncertainties in LCF testing and reduce the variability of between-laboratories lifetime data to within a factor of five. As a result of this work there was an increased awareness of the importance of properly measuring and controlling specimen bending due to misalignment in the load-train in LCF test systems.

Since these studies mechanical testing has progressed, and the use of smaller miniaturised samples has grown in popularity. Within ISO work is underway in ISO TC 164/SC 1 "Uniaxial Testing" to develop "guidelines for Testing Miniaturised Test Pieces". At present within these guidelines there is limited guidance on the effect of misalignment. The work detailed in this report was undertaken to examine the magnitude of the effect on the tensile properties and fatigue life of miniaturised samples under controlled levels of purposely introduced misalignment. In this instance it should be made clear that specimen misalignment refers to misalignment in the loading direction and the test specimen's axial direction.

ETMT TEST SYSTEM

An Instron electro thermal mechanical test machine (ETMT), shown in Figure 1, was used for the practical aspects in the study of the impact of off-axis misalignment on measured mechanical performance. The ETMT [3] is a compact table-top testing system that is ideal for dynamic high temperature testing of smaller samples, capable of easily extending the test regime into extremes of operation, if necessary, to evidence the detrimental effects of misalignment.

The system capability includes [4] ramped or cyclic exposure of both load and temperature; current (ohmic) heating to generate high sample temperatures and high heating/cooling rates and a high integrity enclosure which allows heating experiments to be conducted in air, vacuum or a selected gas environment (usually inert argon). A dynamic load limit of 3 kN, static load limit of 2 kN, displacement limits of ± 5 mm, mechanical loading rates up to 1000 N/s, load cycling frequency of up to 100 Hz and 10 kHz maximum data capture rates provide a

wide-ranging flexibility for whichever test settings might be considered necessary to highlight the effects of sample misalignment from the loading axis.

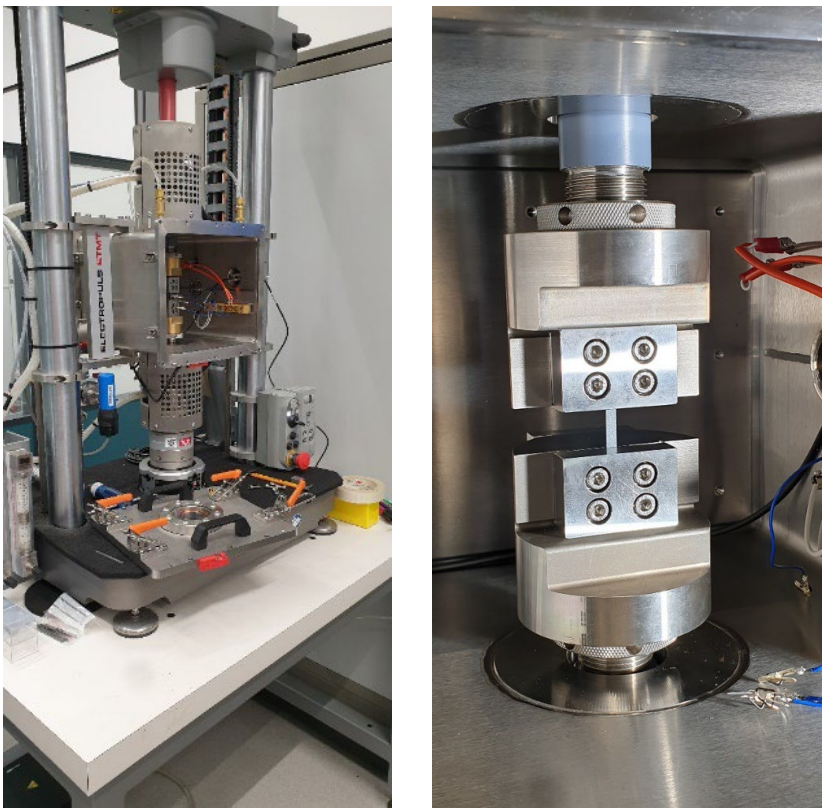

Figure 1 ETMT system and sample installed ready for off-axis testing.

MATERIALS AND SAMPLE DESIGN

The material selected for the test assessments was the certified reference material nickel-based alloy, Nimonic 75, the performance of which has been widely studied and is well-documented in the literature [5]. The typical full stress-strain curve is shown in Figure 2.

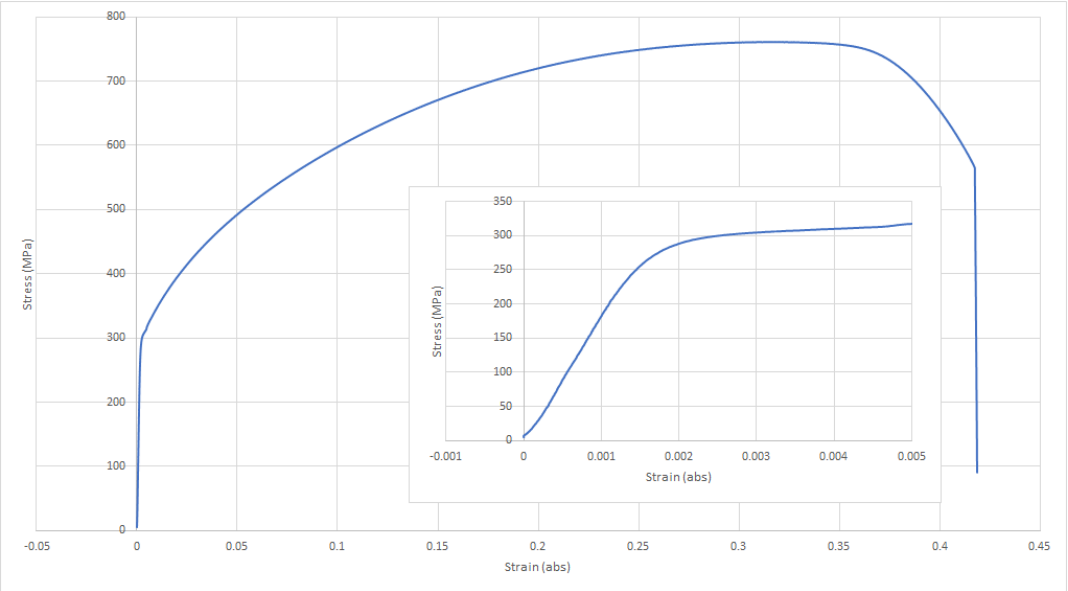

Figure 2 Typical stress-strain curve to failure for Nimonic 75 alloy and magnified elastic/yield region (inset).

Typical ETMT samples are ground rectangular strips, 4 x 1 x 65 mm with a free/ungripped gauge length of 16-20 mm, and these dimensions were used as the basis for the test specimens in this case. Because of the limited load/displacement capacity of the ETMT system, failure properties of the straight-sided sample strips could not be determined, without modification, only properties in the elastic and yield region could be measured. In order to demonstrate the effect of the off-axis loading angle on the failure values of the test specimen, a limited number of waisted geometry samples were produced, which could be extended across all samples should this prove useful. This modified geometry is shown in Figure 3. Samples were waisted down to a parallel gauge length of 7 mm and a gauge width of 1.5 mm, reducing both failure load and displacement comfortably to within system limits.

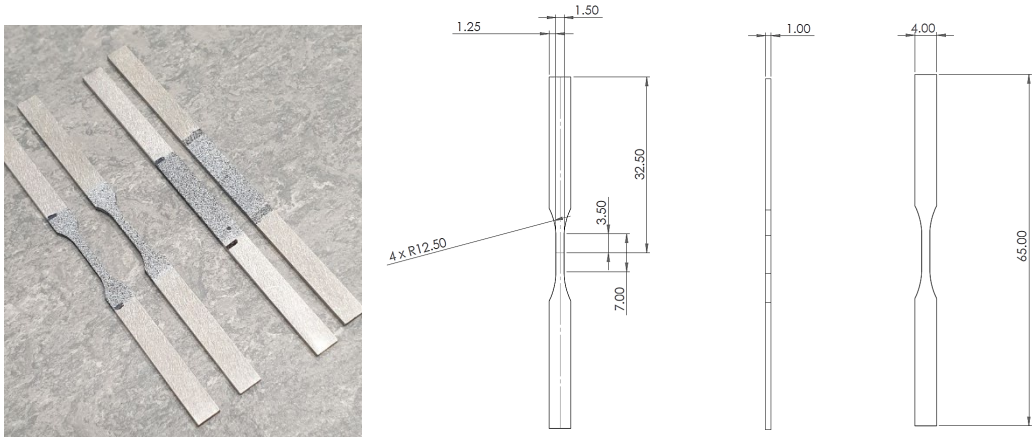

Figure 3 Waisted sample geometry for failure trials in off-axis static tension.

RIG GRIP DESIGN

A new grip design, shown in Figure 4, was required to accommodate and effectively control the orientation of samples rotationally offset from the principal loading axis. Therefore, the entire rig comprising the machine holding bracket, back plate and grips had to be widened accordingly. Finite element modelling suggested effects would be seen at off-axis angles as low as 4° from the vertical and so this was selected as the maximum deviation angle for the design.

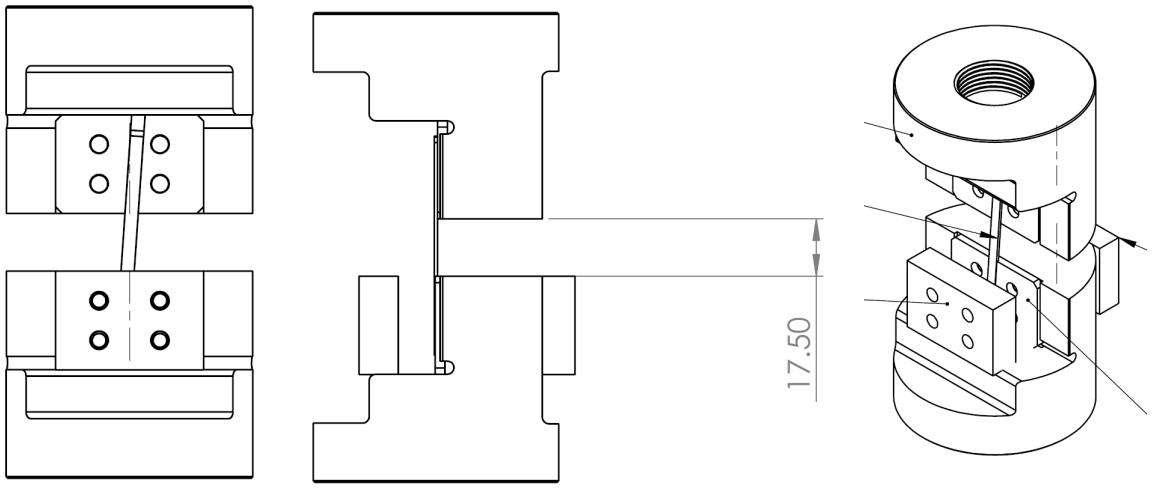

Figure 4 Full rig design showing slotted support back plates and front sample clamping plates.

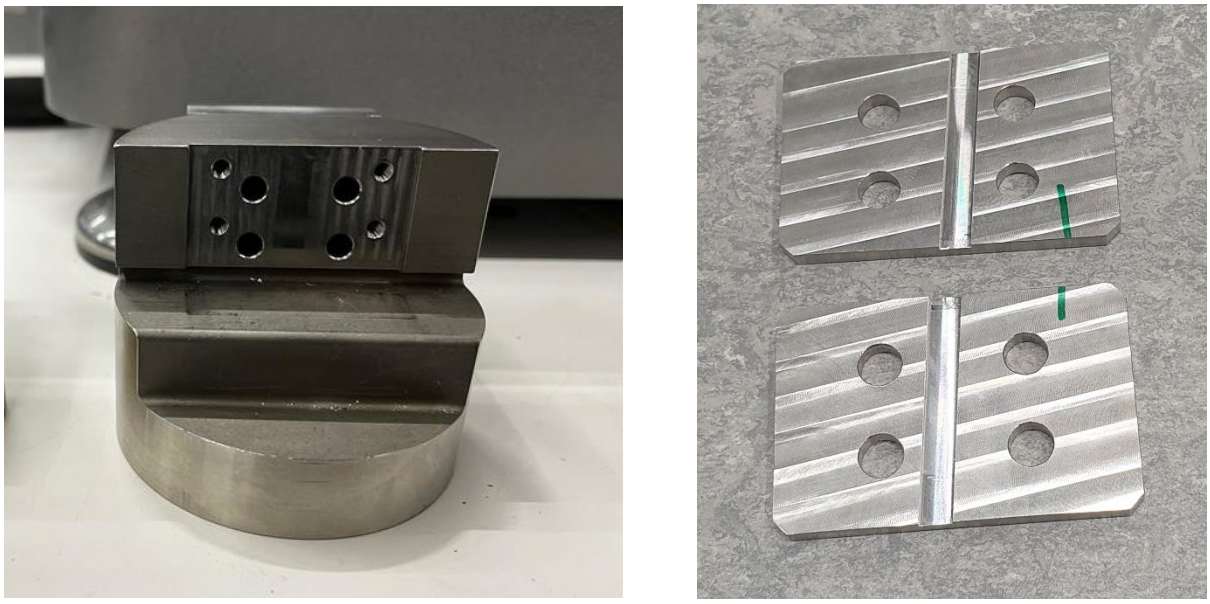

Figure 5 Image of one half of grip manufactured test rig and example of pair of matching coaxially aligned slotted support plates (4° shown here).

Grips were designed for angles: 0°, 0.25°, 0.5°, 0.75°, 1°, 1.5°, 2°, 2.5°, 3° and 4°. All grips, machine holding brackets and back plates were made from stainless steel, suitable for high temperature testing and minimising corrosion or degradation of the rig over time.

The new parts were designed using Solidworks and based on the original ETMT test rig grips. It required careful planning to ensure that everything would fit together, and it was important to keep the samples central to the loading axis and evenly gripped at both ends to prevent early sample failure.

A minor modification was developed after the initial grip manufacture was complete as early trials showed that the precision dimensioning and alignment required to slot the specimen snugly into the collinear angled grooves, machined on the upper and lower gripping plates, was almost impossible to achieve in practice once mounted in the test machine. This resulted in the ground finish 4 mm wide x 0.7 mm deep grooves becoming coaxially mismatched once installed into the two halves of the ETMT rig. This was due to the accumulation of acceptable build tolerances in each individual component, causing problems if misaligned even by as little as 20 µm. It was decided that one end of the alignment plates would be widened to a broad slot, shown in Figure 6, freely accommodating and securing whichever off-axis angle was required by the second plate of the pair. This reduced unwanted friction during testing and localised pinching/bending stresses on the sample which could initiate early failure and proved more reliable when testing.

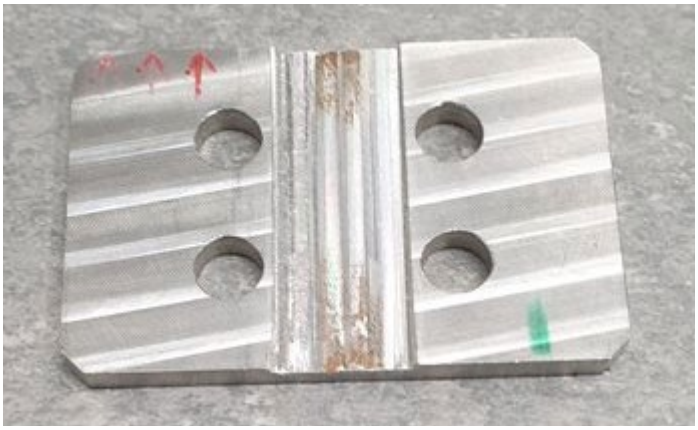

Figure 6 Modified support plate to accommodate all angle offsets, comprising one half of each support plate pair.

STATIC TESTING AND DIC FULL-FIELD STRAIN MEASUREMENT

Initially testing was performed in static tension in conjunction with 2D digital image correlation (DIC) to determine the effect of misalignment on the strain field present in the samples and on the measured mechanical properties with increasing angular offset. The test setup with DIC camera and additional surface illumination are shown in Figure 7

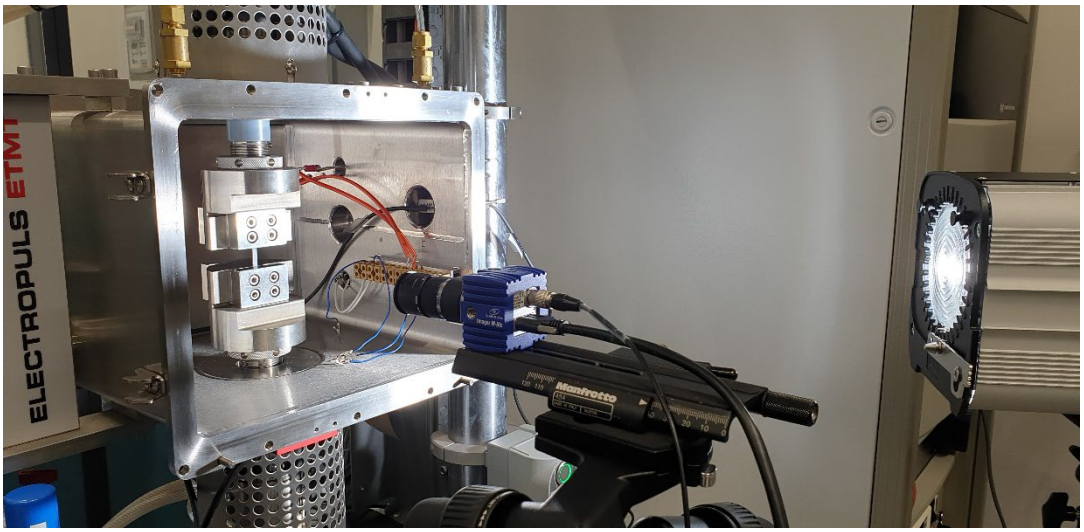

Figure 7 Sample setup for static tensile testing and DIC strain monitoring.

Before mounting, the samples were lightly sprayed with black and white paint to generate a fine speckled random pattern with high contrast but low specular reflection, ideal for DIC monitoring and analysis. An example of this finished surface is shown in Figure 8.

Figure 8 Speckled surface ready for DIC testing, shown magnified.

For DIC monitoring, the camera was set up to avoid obvious artefacts in the image field (dust particles on lens or CCD) during capture which could create strain anomalies in the strain map. This was achieved by observing the image captured against a uniform/white background to detect the artefacts. Examples of this effect are shown in Figure 9.

The strain map captured for each sample was analysed using either a virtual strain gauge (measures average strain over a designated area) or a virtual extensometer (measures the strain between two selected points at either end of the extensometer length.

A large area virtual strain gauge over the full sample gauge length/width was employed in all cases, for the straight-sided samples - this covered the whole sample area visible to the camera, for the waisted samples - this included only the narrowed parallel region at the centre. In addition, for the straight-sided samples, virtual strain gauges and extensometers monitoring only the central region of the sample (away from the influence of the grips), orientated either parallel to the loading axis or parallel to the sample were analysed to generate stress-strain curves for each test where possible. Examples of these constructions are also shown in Figure 9. In particular for the waisted samples with severely reduced width and gauge length, there was insufficient space in the gauge area to successfully analyse strain oriented in line with the loading axis or to sensibly consider a reduced central section.

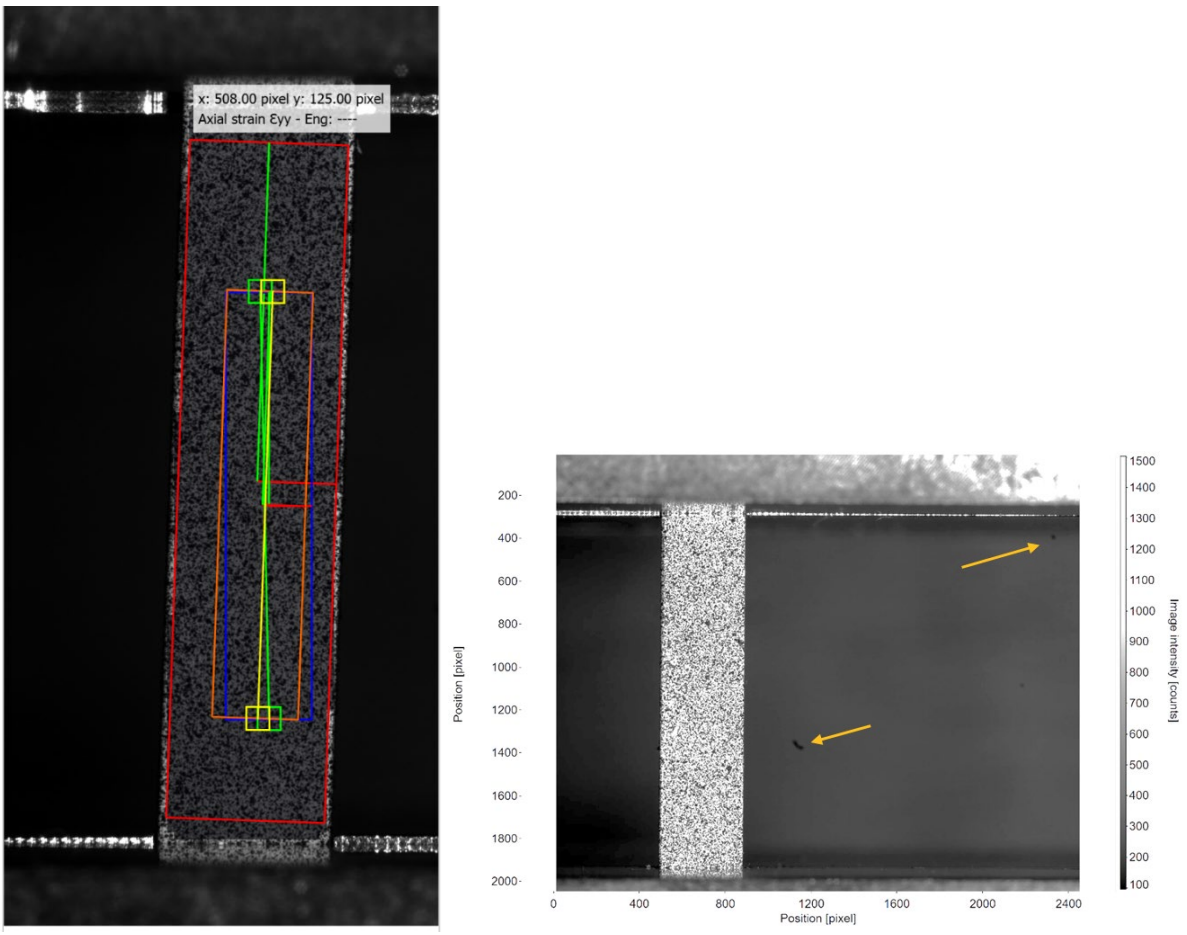

Figure 9 Virtual strain gauges (rectangular regions) and virtual extensometers (straight lines) applied to a test specimen during DIC analysis (left) and stationary artefacts in the DIC camera image avoided by careful image field location of the specimen (right).

Possible errors in the DIC results/setup could arise from various sources including:

- Orientation of camera to loading axis and/or sample
- Orientation and precise locating of virtual gauges and extensometers
- Low sampling rates needed to minimize image capture data volume
- 2D setup with a single camera – any out-of-plane deformation of the sample during test is interpreted as an in-plane effect
- For high strains, speckle coating cracks/splits/flakes, limiting accurate range of monitoring
- Unavoidable marks on lenses or CCD sensors cause glitches in the correlation analysis.

Straight-sided specimens were tested at all available offset angles, advancing into the plastic regime but not fully to failure in order to keep the ultimate static load reached in the tests below 2 kN. Waisted specimens were tested only at the angle extremes and the centre of those available, i.e. 0°, 2° and 4°, and these specimens were loaded all the way to complete failure/rupture.

STATIC TENSILE AND DIC RESULTS

Images of the typical specimen residual deformation visible after testing are shown in Figure 10 for the offset angle extremes of both straight-sided and waisted specimen geometries. These show significant lateral deformation after the plastic transition as the sample aims to align itself to the loading axis for the angle offset examples but no change in the failure mode or location for those tests where failure was achieved.

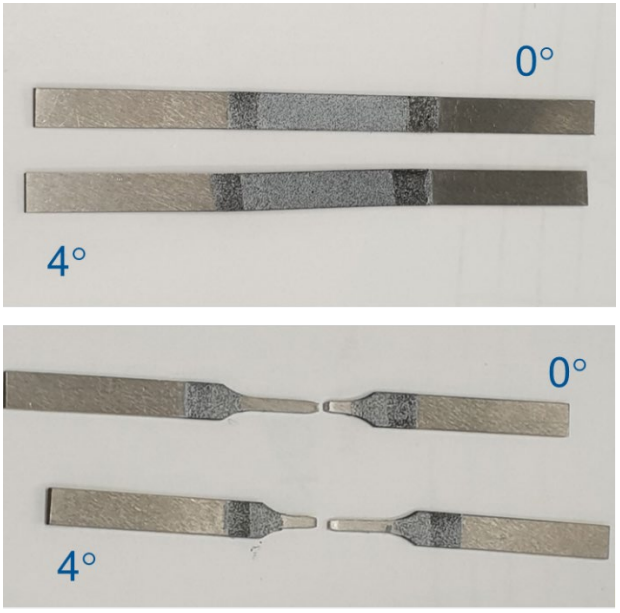

Figure 10 Typical failures and post-yield permanent lateral deformation for aligned and off-axis samples, both straight-sided and waisted geometries.

Stress vs. displacement traces for all straight-sided and waisted specimen geometries at the tested off-axis angles are given in Figure 11 and Figure 12, respectively. These showed mostly similar behaviour between all the offset angles with no clear trend with increasing offset.

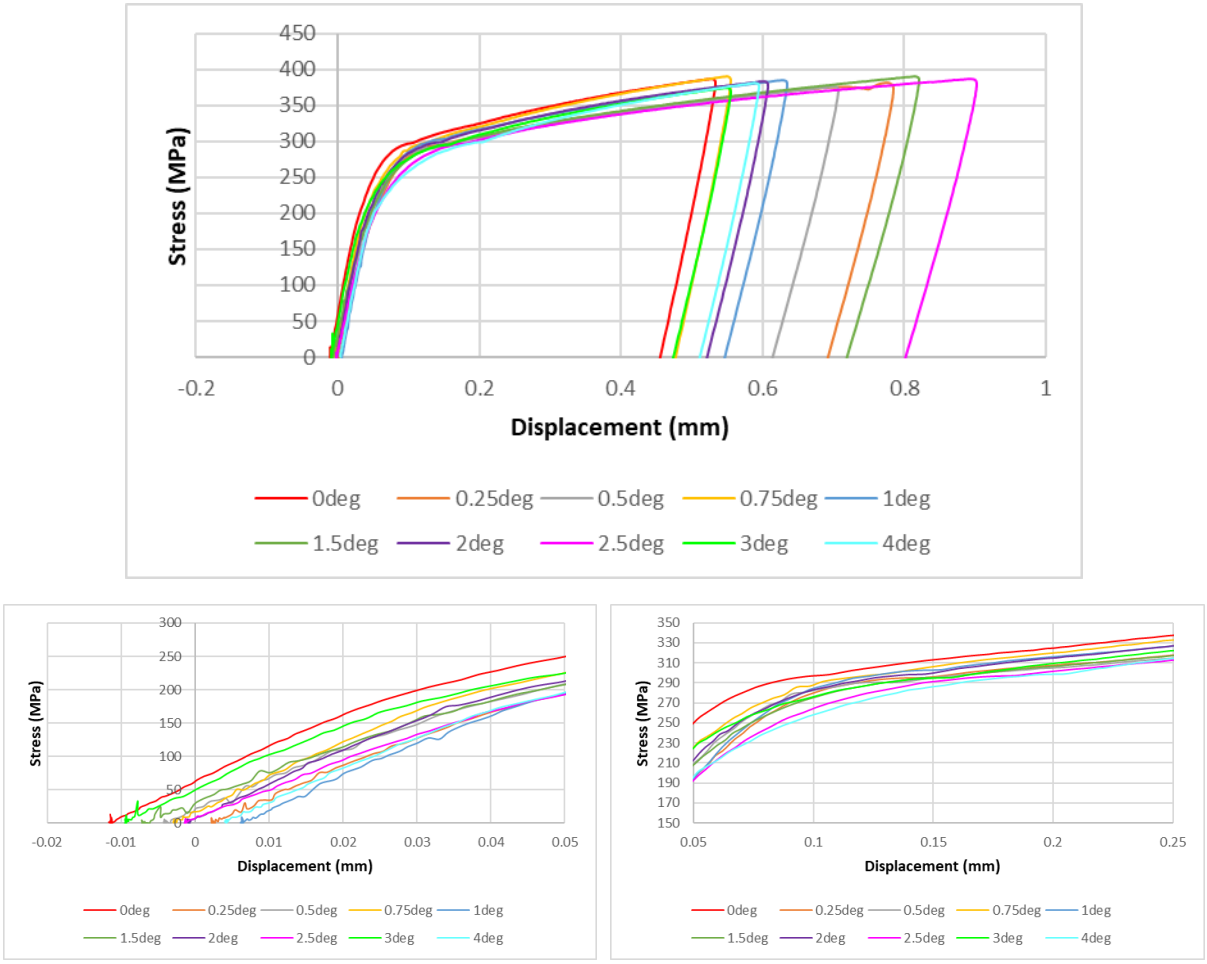

Figure 11 Stress/displacement results from straight-sided specimens at all angles, tested to <2 kN, mechanical test machine data only (above) with magnified regions for elastic (left) and yield (right) response.

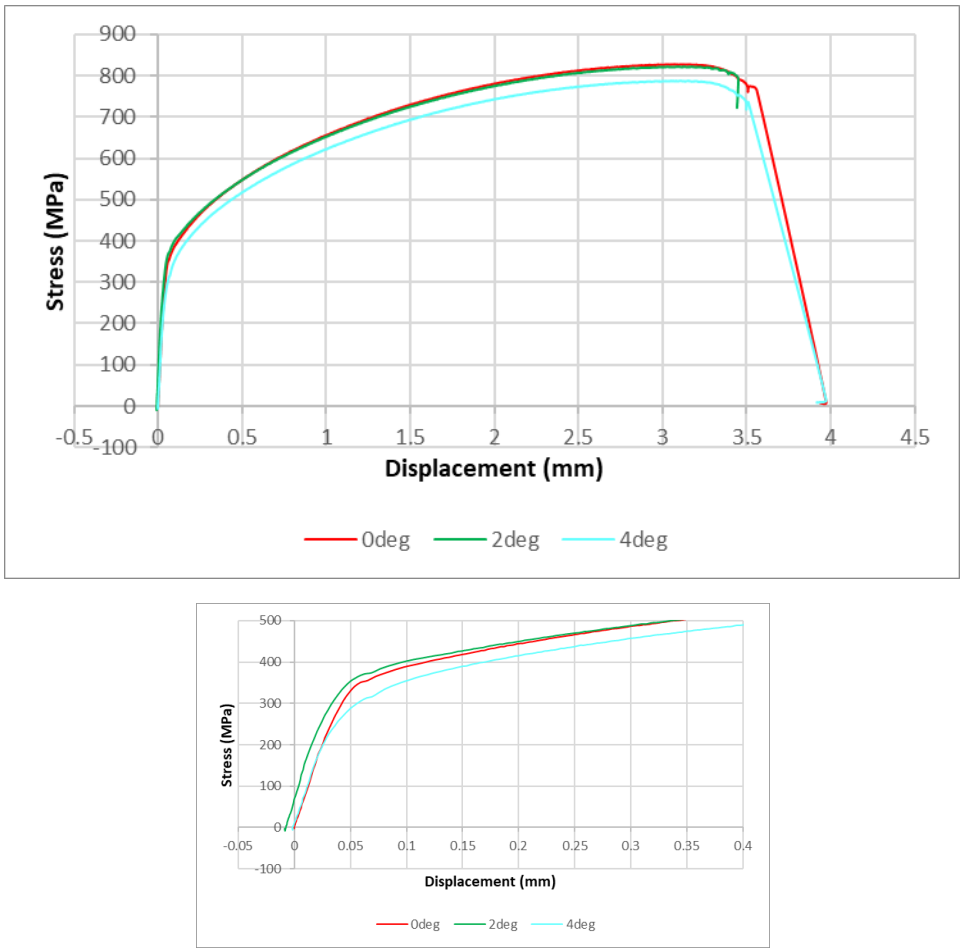

Figure 12 Stress/displacement results from waisted specimens at selected angles, tested to failure, mechanical test machine data only (above) with magnified region for elastic and yield response (below).

The strain maps for all the straight-sided and waisted samples are shown in Figure 13 and Figure 14, respectively. The data are mostly indistinguishable at low strains (0.1%) and increase in strain field asymmetry with increasing angle and strain. It is also clear that the extensions reached for a full test to failure results in premature speckle coating failure, seen in the waisted samples at high strain levels. The results from this point are therefore less reliable, despite employing a differential strain analysis between consecutive images rather than a cumulative strain analysis determined from an initial reference image to minimise the effect of the coating failure on the processed strain results.

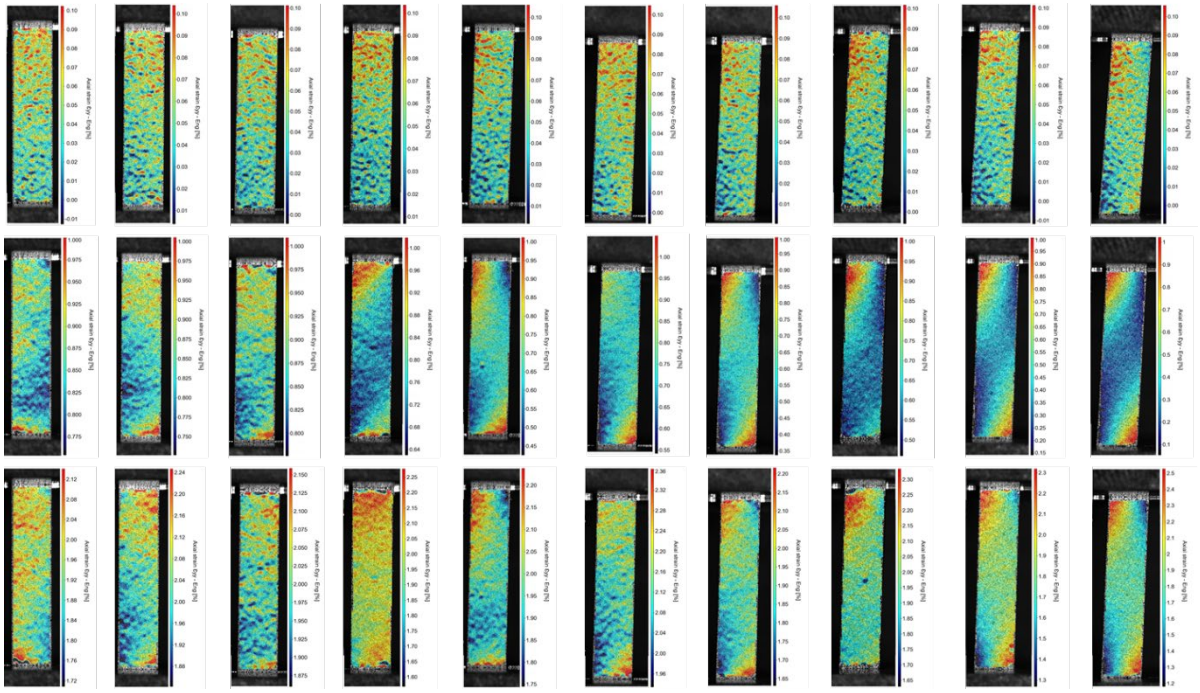

Figure 13 Full-field strain maps for straight-sided specimens generated using DIC for all off-axis test angles in increasing order starting from 0° to 4° (left to right). The rows represent snapshots taken at 0.1% (upper), 1% (mid) and ~2% strain (lower).

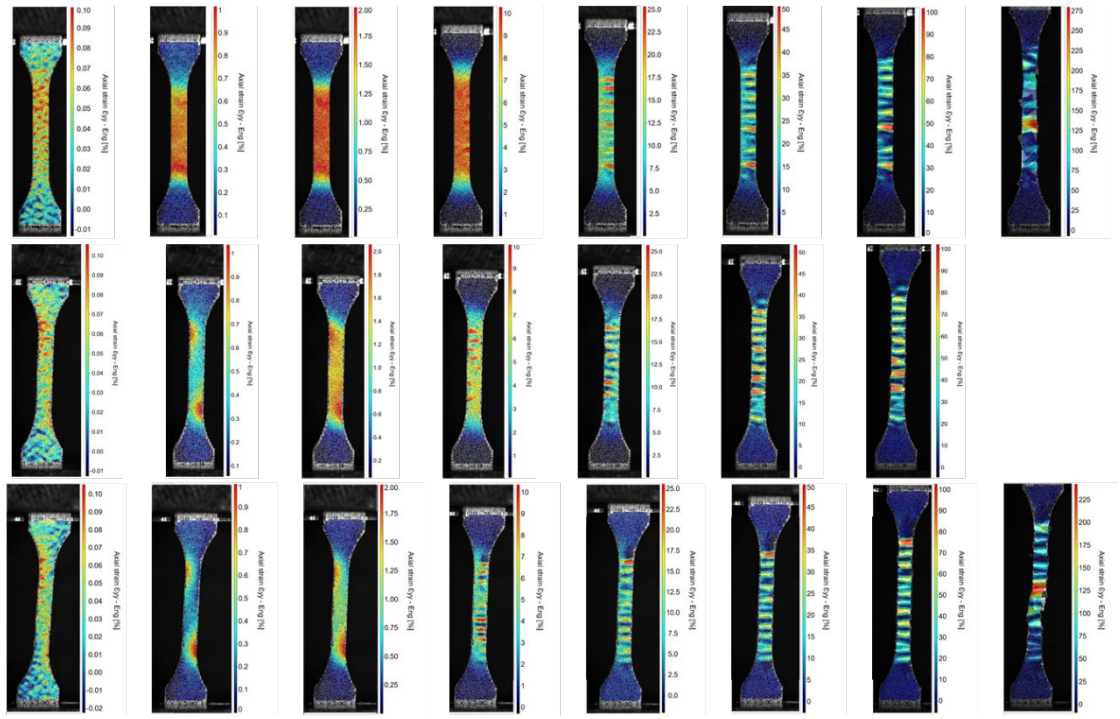

Figure 14 Full-field strain maps for waisted specimens generated using DIC for 0° (upper row), 2° (mid row) and 4° (lower row) in order of increasing strain 0.1, 1, 2, 10, 25, 50, 100% and at failure (left to right).

The effect of the orientation/averaged area/nature of the strain analysis for the straight-sided samples (virtual strain gauge or extensometer) is shown in Figure 15. This clearly indicates that all stress-strain curves overlapped exactly and so the strain asymmetry did not affect the measured sample strain from which the mechanical properties were calculated. Evidence for this insensitivity of the static tests to the strain concentrations/asymmetry can also be seen in the mechanical data summary in Table 1 and also in the nominally identical stress-strain curves for all tested angles shown in Figure 16. The data analysis applied to the stress-strain curves to extract this data is provided in Figure 17.

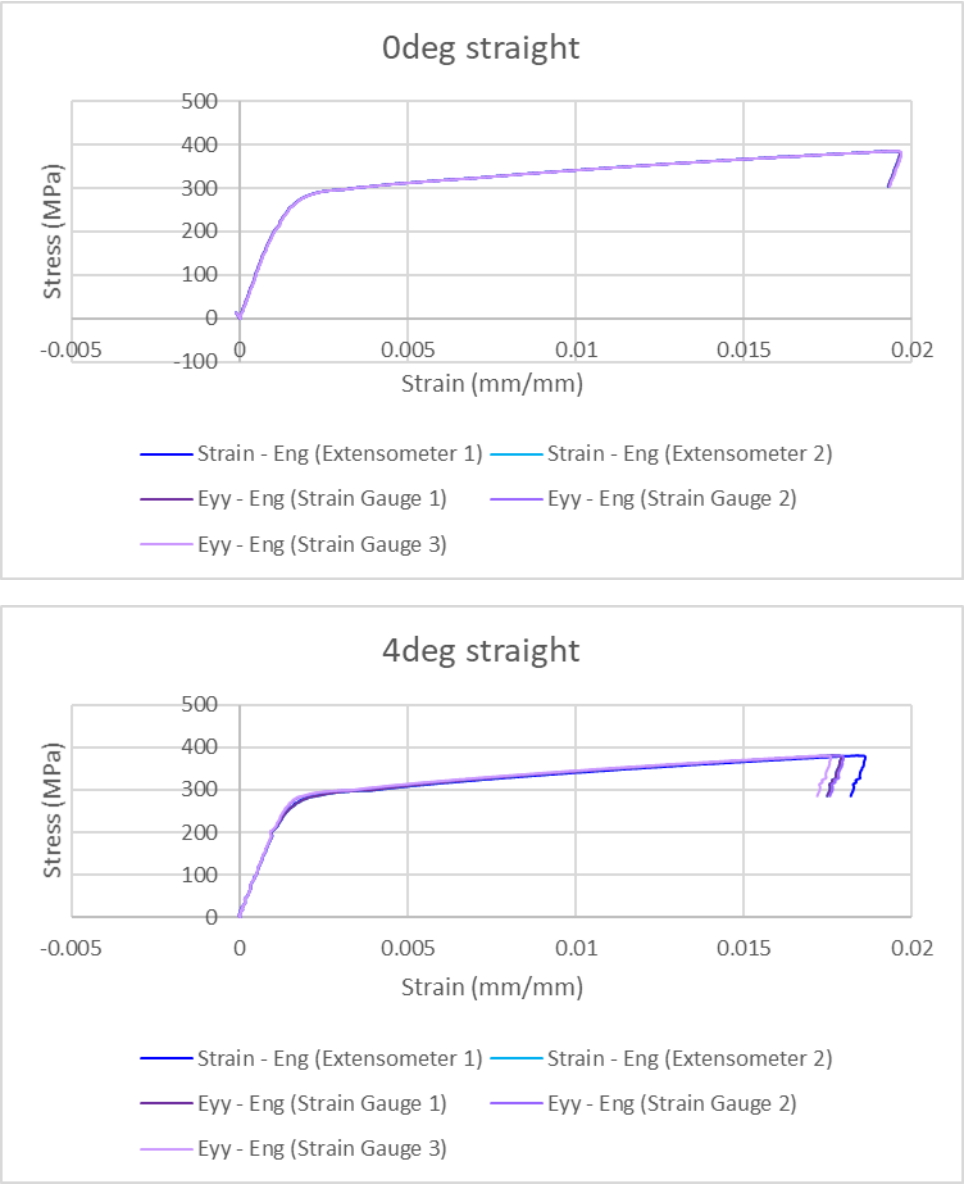

Figure 15 Comparison of stress-strain curves for different DIC post-processing analysis routes for angle extremes of 0° (above) and 4° (below) only.

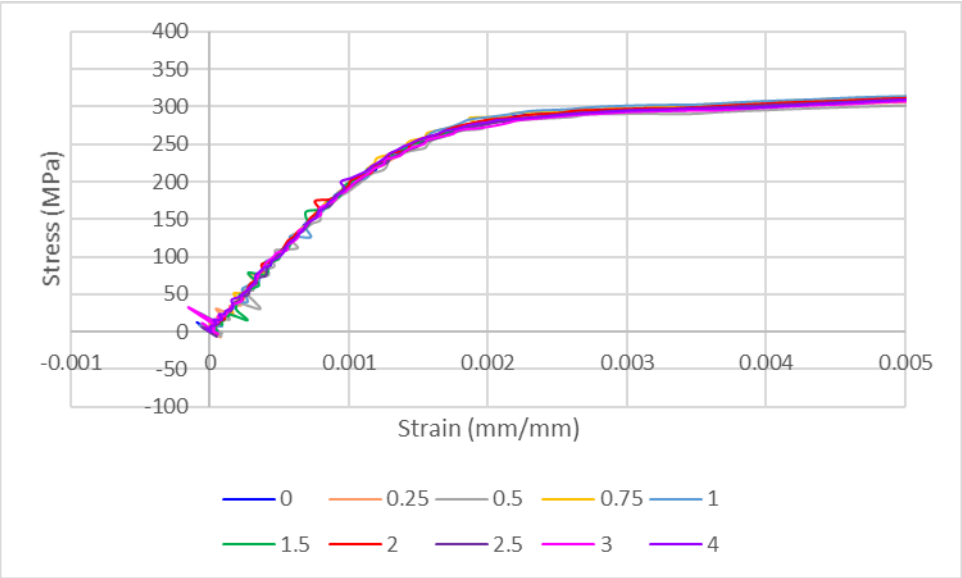

Figure 16 Comparison of average strain using the full sample area virtual strain gauge for straight-sided specimens at all tested angles.

Table 1 Summary of static tensile properties for straight-sided and waisted samples at all tested angles.

Sample ID	Angle (degrees)	Sample type	0.01-0.075% modulus (GPa)	0.2% yield stress (MPa)	Maximum tensile stress (MPa)	Stress at failure (MPa)	Elongation to failure (%)
ajap019	0	straight	201.00	296.44			
ajap020	0.25	straight	189.57	296.57			
ajap012	0.5	straight	197.76	290.23			
ajap022	0.75	straight	202.95	303.85			
ajap014	1	straight	199.67	304.72			
ajap021	1.5	straight	206.78	297.58			
ajap017	2	straight	201.99	301.22			
ajap023	2.5	straight	195.65	298.55			
ajap015	3	straight	195.97	297.78			
ajap013	4	straight	198.75	300.13			
ajap007	0	waisted	208.17	355.5	828.6	767.0	36.5
ajap004	2	waisted	225.06	373.4	822.4	781.0	36.3
ajap003	4	waisted	192.1	313.5	788.0	721.5	37.5

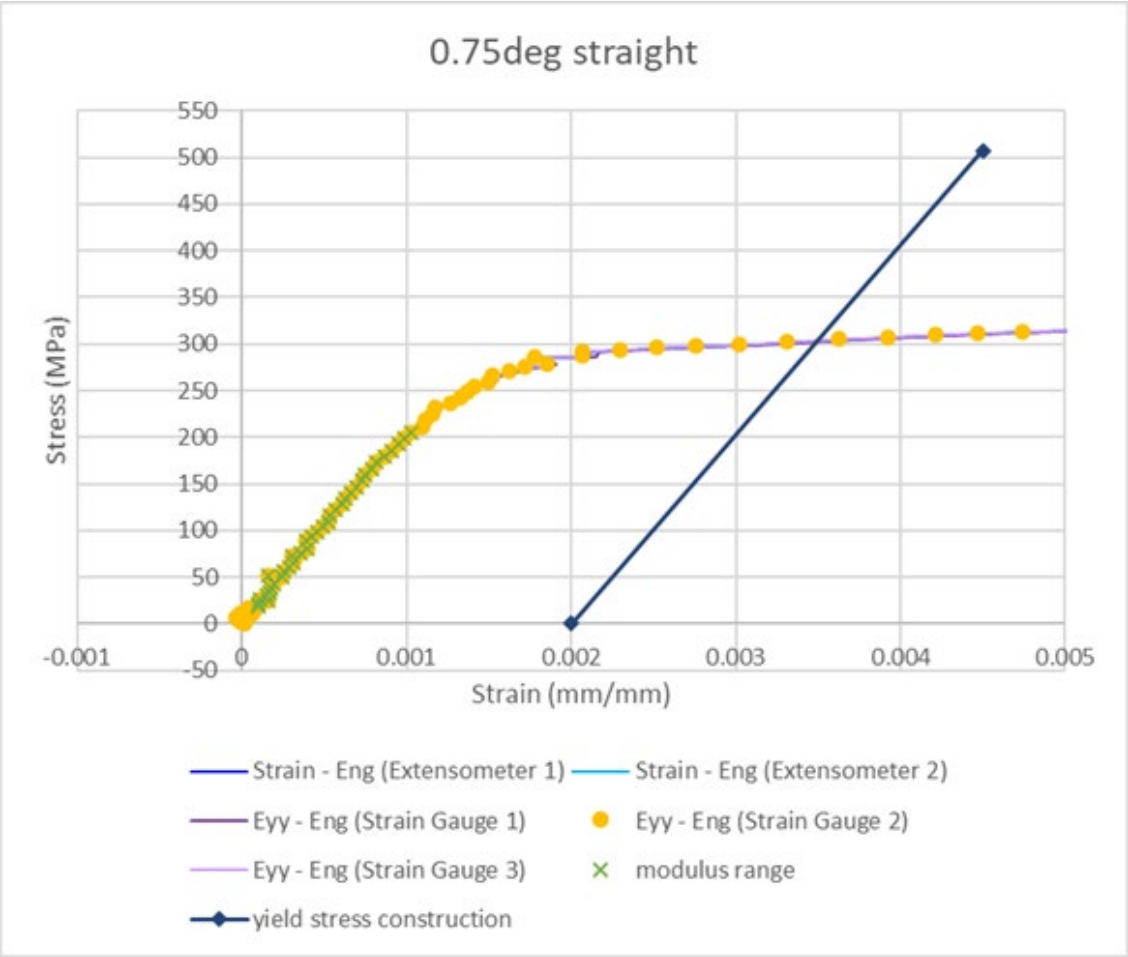

Figure 17 Elastic /yield calculations and constructions from the stress-strain curve for each test specimen, 0.75° straight-sided specimen example shown here with linear response strain range highlighted for modulus determination and the crossover between 0.2% offset line (parallel to modulus slope) and the specimen stress-strain curve indicating the 0.2% proof yield stress.

The same effect can be observed for the waisted samples, although in this case there is more scatter in the resulting data with angle offset.

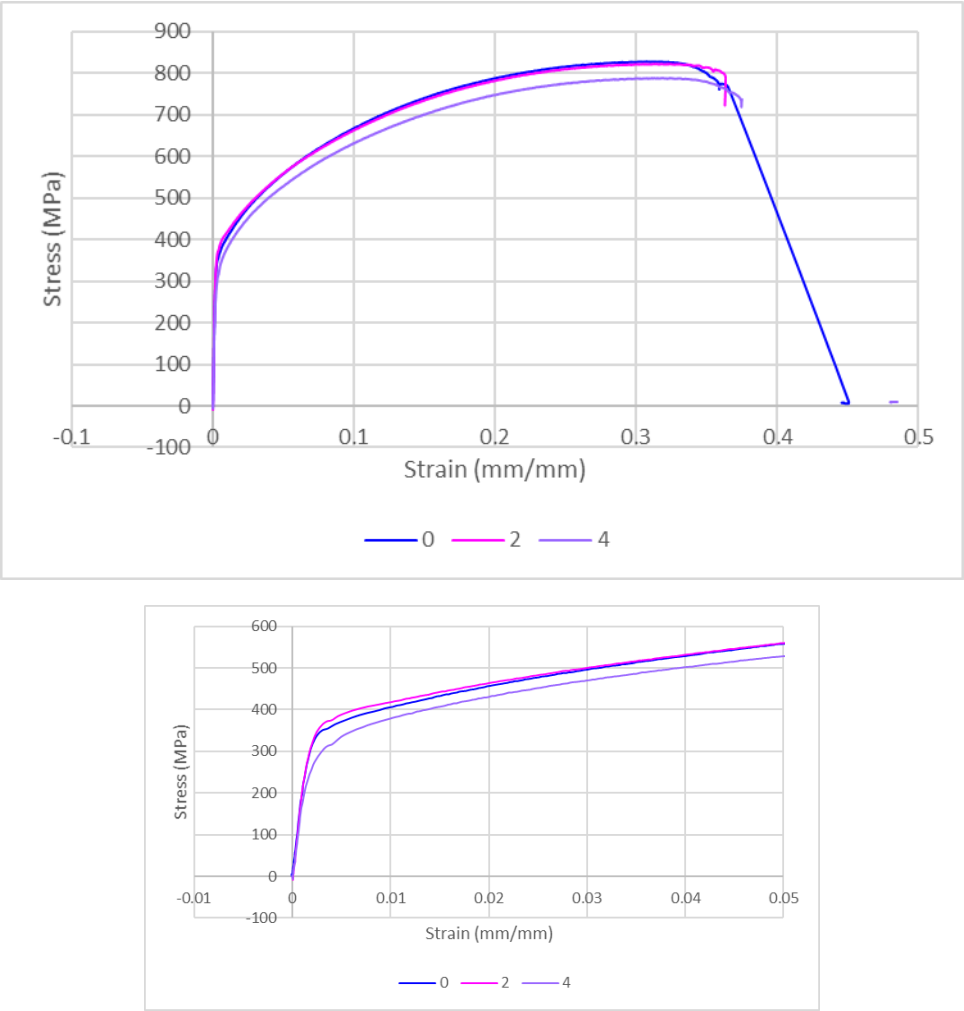

Figure 18 Comparison of average strain using the full sample area virtual strain gauge for waisted specimens at selected test angles (above), magnified elastic and yield region (below).

Finally, the elastic and yield properties for all the tested samples are plotted in Figure 19, showing no clear trend in the measured properties with increasing angle.

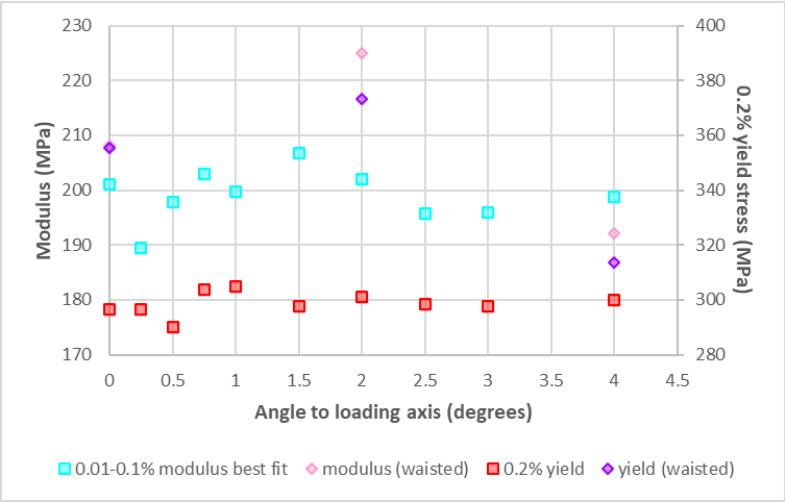

Figure 19 Plot of elastic modulus and 0.2% yield stress for both sample geometries with angle relative to the loading axis.

Issues potentially influencing the absence of a clear trend in static mechanical properties with increasing offset angle may include:

- Clearance on angle slotted support plates in rig, bolt holes for clamping, and width of milled angle slots could allow some errors in specimen orientation outside the expected values
- Widening of the specimen slot on one support plate of the pair may permit some realignment/accommodation or slip during the loading process itself
- Thickness chamfers in the sample affect the clamping load at either end which may have a greater effect on measured properties than the offset angle
- Inherent material variability may have a larger effect than potentially subtle variations caused by small angle offsets
- The effect of small angles is expected to be small and may simply be lost in cumulative uncertainties in the static testing
- Monotonic loading is generally less susceptible to showing large effects from misalignment when compared to cyclic fatigue testing where the cumulative effect of bending strains over multiple loading cycles has been shown to exhibit a more substantial effect.

In conclusion, the static test programme was useful to demonstrate the effects on the strain field caused by off-axis loading but the observed strain asymmetry is relatively localised and, in static testing at least, may not necessarily produce consistent or observable numerical effects on property values as the evidence above suggests.

The next stage was to consider dynamic fatigue testing where cumulative cycles of load may highlight the detrimental effects of localised strain/stress concentrations.

DYNAMIC FATIGUE TENSILE TESTING

Fatigue testing was carried out using the straight-sided specimens for selected angle offsets; 0°, 2° and 4°. Testing was limited because of the longer test durations involved in fatigue testing. Samples were tested at maximum stresses of 75% UTS equivalent to 610 MPa, 65% UTS equivalent to 488 MPa, and 50% UTS equivalent to 407 MPa with 2-3 samples tested at each angle and stress level combination, depending on the consistency of the results. The test frequency used was 5 Hz with R = 0.1. All samples were tested to failure and the cycle count to failure plotted against maximum stress for each angle offset.

DYNAMIC FATIGUE TENSILE RESULTS

All the tested samples failed near the edge of the upper/moving grip shown in Figure 20a and b. The cycles to failure for different maximum stresses were plotted as an S-N curve presented in Figure 20c. Comparing the fitted (logarithmic) curves shows that the sample fatigue life decreases as the misalignment angle increases. The individual data points are provided in Table 2.

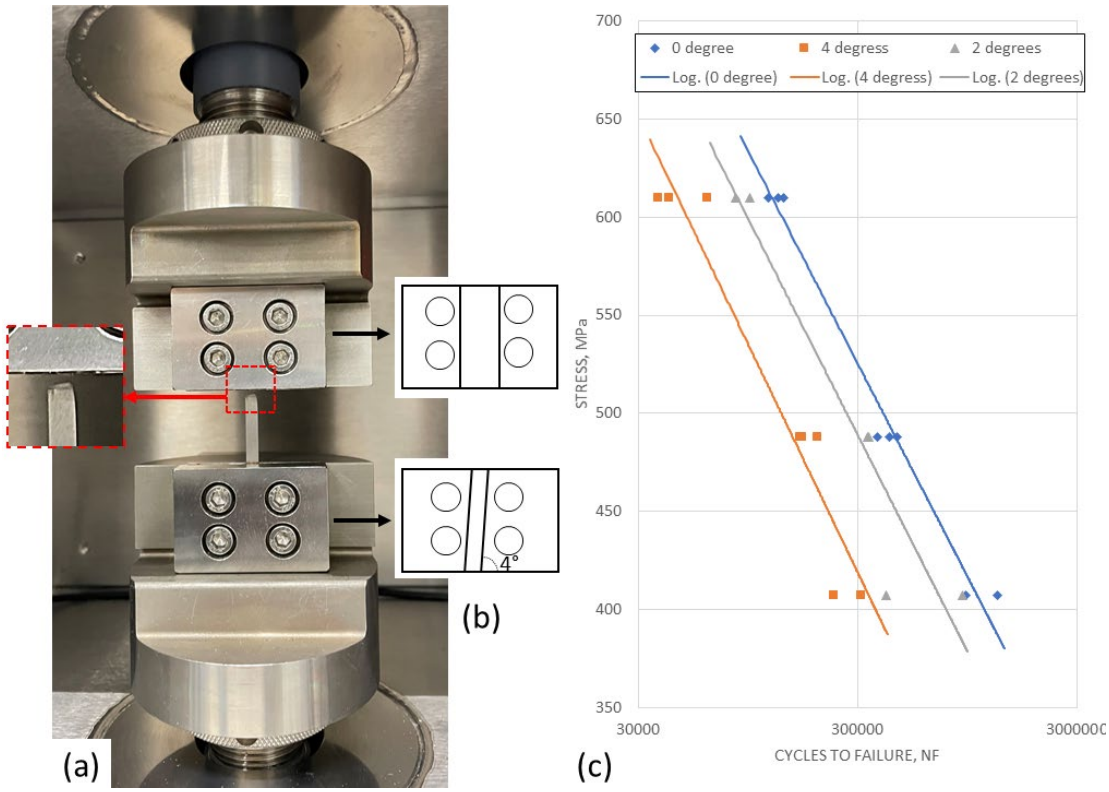

Figure 20(a) The test setup with a sample after being cycled to failure using (b) 4° misalignment fixture. (c) Number of cycles to failure using different stress amplitudes, i.e. S-N curves for each misalignment angle. The quality of the fitting (R2) for all lines is better than 90%; however, R2 is meant to describe linear fitting and might not represent the quality of fitting for non-linear relationships.

Table 2 Summary of fatigue test data.

Maximum Stress (MPa)	Cycles to Failure		
	Offset angle		
	0°	2°	4°
610	138,667	83,508	36,907
	129,911	96,829	61,715
	117,750		41,634
488	452,996	332,772	198,043
	370,582	339,124	164,002
	418,210		167,528
407	933,537	900,463	233,889
	1,296,829	403,503	310,626

DISCUSSION

The centre lines of the ideally-rigid grips are offset laterally with respect to each other by an amount ‘e’ that is proportional to the material’s ability to deform plastically. Unlike the angular offset (Figure21a), in this case, bending will vary along the length of the sample, both in magnitude and sign. The cross-section at the middle of the gauge length will remain neutral, and no bending will take place at this location. But this ignores the two parts of the problem: (1) loading the samples in tension, which introduces bending as the sample aligns itself to the load, which means – given the non-uniformity of the stress distribution – a different part of the sample is experiencing a different stress state that does not equal the expected stress in an aligned sample, and (2) this is worsened during fatigue cycling. As a result, a mix of bending and torque moments are present during the fatigue cycling, localising the strain on one side of the sample. This (minimal) localisation exacerbates during the test, which shortens the sample fatigue life. Thus, the test data include the additional bending strain superimposed on the axial strain.

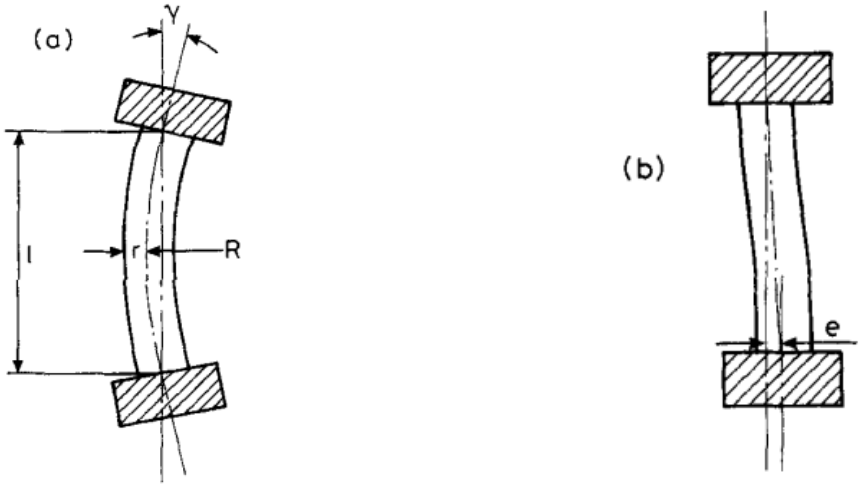

Figure 21 Bending mechanisms due to load misalignment in fatigue test systems (a) Angular offset, (b) Lateral offset [4].

Within this work we have introduced misalignment of 2° and 4° to evaluate the effect this would have on the fatigue life of miniaturised samples designed for the ETMT. Scholz has previously demonstrated that for full-scale LCF tests an applied bend strain can dramatically reduce the number of cycles to failure as shown in Figure 22.

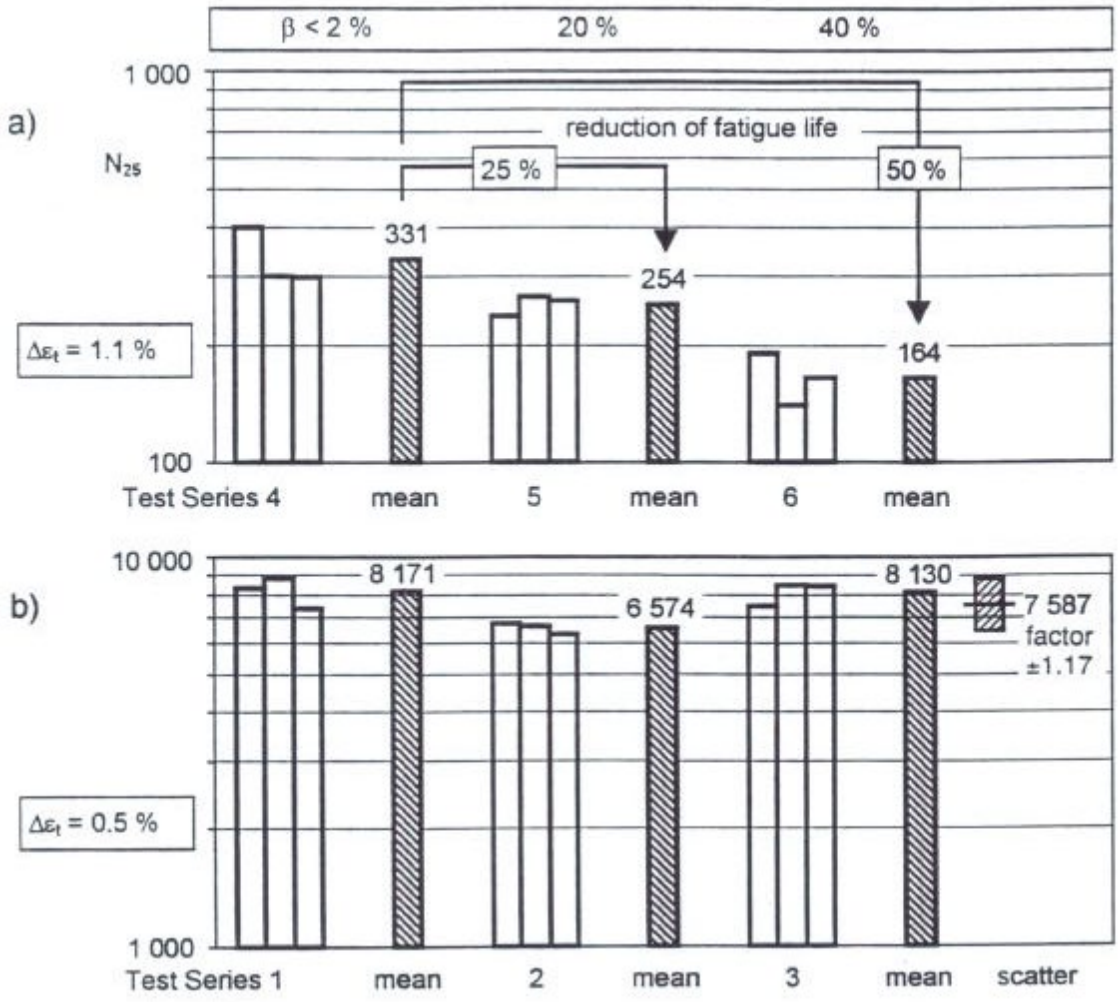

Figure 22 Comparison of fatigue life under different levels of specimen percent bending [6].

Analysis of these results shows there to be a nominally linear relationship between the reduction in fatigue life and the applied bending strain through sample misalignment, Figure 23.

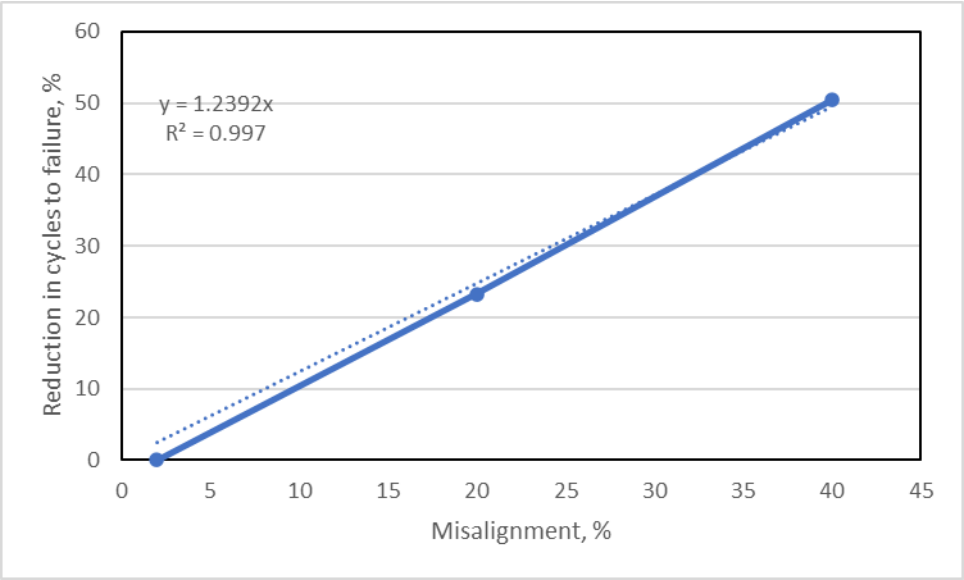

Figure 23 Reduction in fatigue life as a function of misalignment for the data of Scholz as reported in [6].

A similar analysis has been conducted on the fatigue data for the miniaturised ETMT samples reported here. This shows a similar effect on the reduction of fatigue life, in this case presented as degrees misalignment rather than as %bending. This is shown in Figure 24, where a straight-line fit has been used based on the average of the three curves for the different applied stresses.

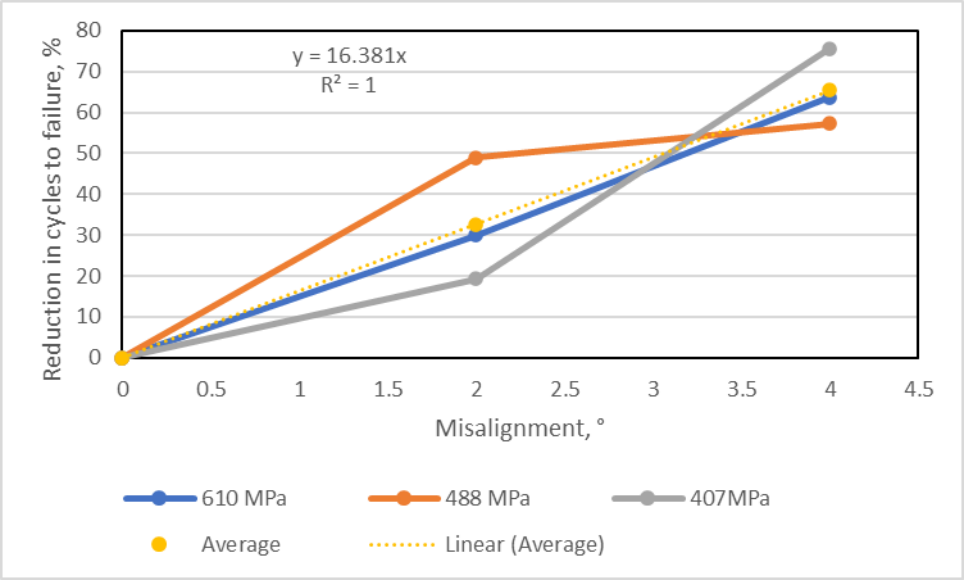

Figure 24 Reduction in fatigue life as a function of misalignment for the miniaturised ETMT samples.

Whilst a similar effect has been demonstrated on the fatigue life, under large scale sample LCF testing the bending and misalignment can be relatively easily measured and corrected for with alignment cell fixtures, as described in [7]. This does not readily translate to miniaturised test specimens, whether they are flat tensile dog bone geometries, small cylindrical samples or the simple ETMT sample geometries used in this work. There is a need for a recognised and

validated method to control specimen alignment for miniaturised specimens which at present does not exist.

CONCLUSION

In conclusion, for fatigue loading load misalignment reduces the number of cycles to failure. This has been demonstrated in previous programmes on large scale test specimens. This has been shown to be due to bending strains in the test piece introduced by actual bending of the specimen and/or test machine misalignment. For large scale test pieces this has been considered in procedures for measurement and control methods and alignment fixtures. However, the read across and application to miniaturised test pieces has not really happened. As the popularity of these scale of tests increase it is becoming of greater importance to introduce the same rigor and control into these tests

[1] G. B. Thomas and R. K. Varma, “Evaluation of low cycle fatigue test data in the BCR/VAMAS intercomparison programme,” Report EUR 14105 EN, BCR Information Applied Metrology, ISSN 1018-5593, Commission of the European Communities, 1993.

[2] F. A. Kandil, “VAMAS Technical Working Area 13 on Low Cycle Fatigue: An Overview of its Work and Achievments”.

[3] B. Roebuck, M. Brooks and A. Pearce, “Good Practice Guide for Miniature ETMT Tests,” NPL Good Practice Guide No. 137, 2016.

[4] Instron, *ETMT_M114025-OP-EN_C,* Electro thermomechanical Test (ETMT) System - Operating Instructions, 2010.

[5] Joint Research Centre - European Commission, “Certified Reference Material Certificate BCR-661B NIMONIC 75 FOR TENSILE PROPERTIES,” October 2015. [Online]. Available: https://crm.jrc.ec.europa.eu/p/q/nimonic+75/BCR-661B-NIMONIC-75-FOR-TENSILE-PROPERTIES/BCR-661B.

[6] F. Kandil, “RECENT INTERCOMPARISONS ON LOW CYCLE FATIGUE AND ALIGNMENT MEASUREMENTS, Report No. 41,” VAMAS ISSN 1016-2186, 2001.

[7] F. Kandil, “A PROCEDURE FOR THE MEASUREMENT OF MACHINE ALIGNMENT IN AXIAL TESTING - Report No. 42,” VAMAS, 2001.

[8] F. Kandil and B. Dyson, “The influence of load misalignment during uniaxial low-cycle fatigue testing - I: Modelling,” *Fatigue and Fracture of Engineering Materials and Sructures,* vol. 16, no. 5, pp. 509-527, May 1993.

APPENDIX

DETAILS OF FEA MODELLING OF MONOTONIC TENSILE TESTS

ETMT ALIGNMENT MODELLING

An Abaqus CAE model was created of the straight sided tensile sample. The sample was partitioned to give a grip region at each end of the sample. The grip regions were 7.5 mm deep. The partitions were defined so that the portioning line would remain horizontal even after the sample was rotated. A large rotation has been applied to the sample in Figure 25 to demonstrate this.

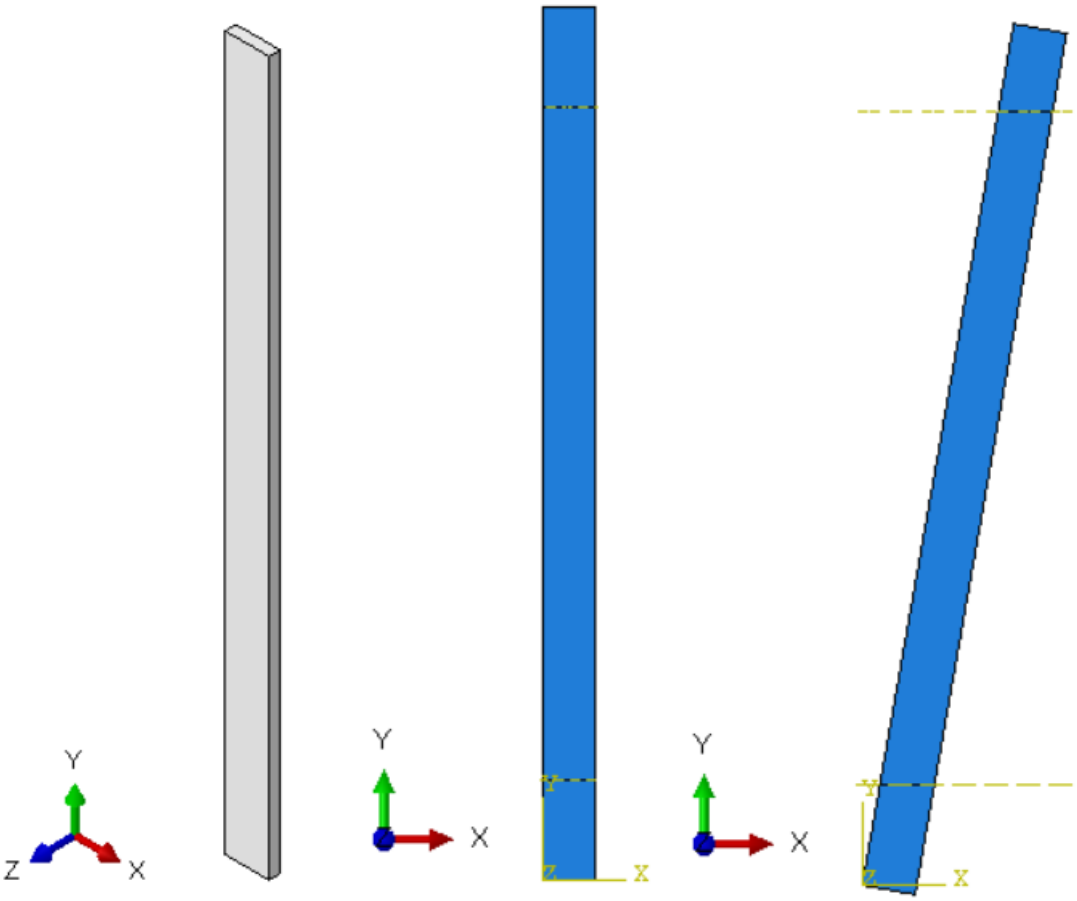

Figure 25 Abaqus CAE created geometry of the tensile sample.

The sample was defined in a vertical orientation initially and was meshed with linear hexahedral elements (C3D8R). Two geometry sets were defined for the top and bottom grips. The bottom grip was fully constrained. The top grip was constrained in the x and z directions, but displaced in the y direction, see Figure 26, which shows loading for the vertical and off-axis samples. To create subsequent models, the geometry was rotated to a set angle (0.25°, 0.5°, 0.75°, 1°, 1.5°, 2°, 2.5°, 3° or 4°) and a new input file created.

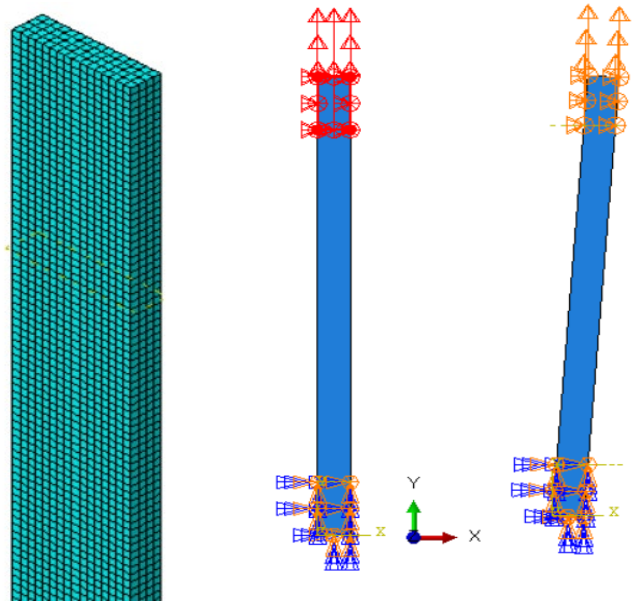

Figure 26 Mesh and boundary conditions applied to geometry.

An FEA model of the waisted tensile samples detailed in Figure 3 was also generated. The sample was meshed, and boundary constraints applied as before. The waisted geometry created is shown in Figure 27.

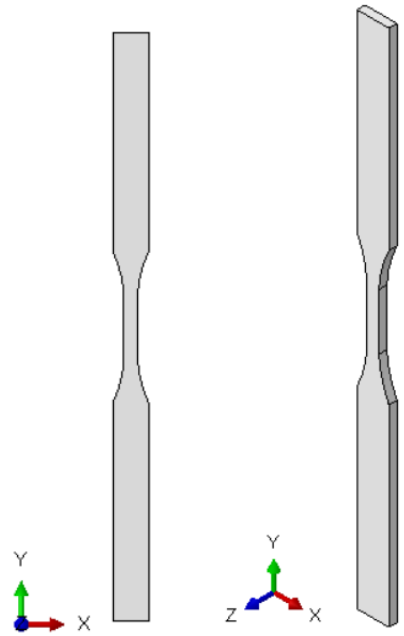

Figure 27 FEA geometry of the waisted sample.

Three different materials were defined within the model using an elastic-plastic material model definition. These consisted of a generic 'hard' steel, a generic 'soft' steel and Nimonic 75, with stress-strain data for all three given in Figure 28. Both used existing steel data, but

one was softer steel than the other. The stress-strain curves are shown below in Figure 28. Appropriate applied displacements were calculated from the elongation to failure ranging from 3.5 mm to 16 mm.

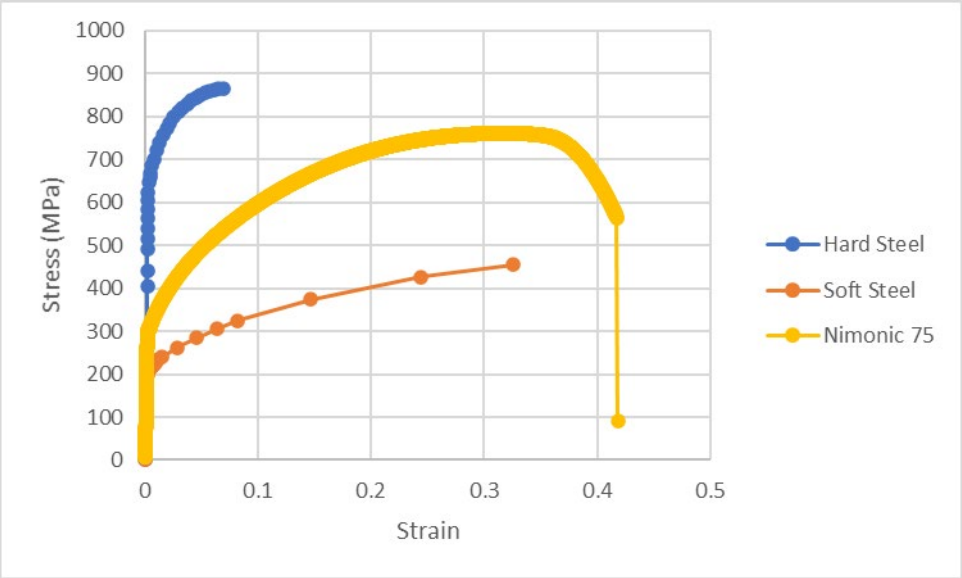

Figure 28 Stress-strain curves for the materials used within the FEA modelling.

Contour plots of axial stress in MPa (S22) and strain (E22) have been obtained from all analysis run. All analyses run with hard steel had an applied displacement of 3.5 mm. For the straight sided samples, the soft steel analyses had an applied displacement of 16 mm and the Nimonic 75 samples had an applied displacement of 5 mm. For the waisted samples these were reduced to 7 mm and 4 mm, respectively.

Figures 29 - 38 show the stress and strain contour plots for straight-sided hard steel samples for the full range of offset angles. Figures 39 - 48 show the stress and strain contour plots for straight-sided soft steel samples for the full range of offset angles, while the Nimonic 75 contour plots are presented in Figure 49 and 50.

For the waisted samples Figures 51 - 53 are for hard steel, Figures 54 - 56 are for soft steel and Figures 58 - 60 are for Nimonic 75. In the case of the Nimonic 75 contour plots, Figure 58 and Figure 60 show plots with tighter contour limits which shows more detail in the stress/strain distributions. Plots with tighter contour limits have also been produced for straight-sided and waisted samples with hard and soft steels. The aligned and 4° offset cases were selected and the contours were plotted at the last displacement where the sides in the central region of the sample were still straight, Figures 61 - 64.

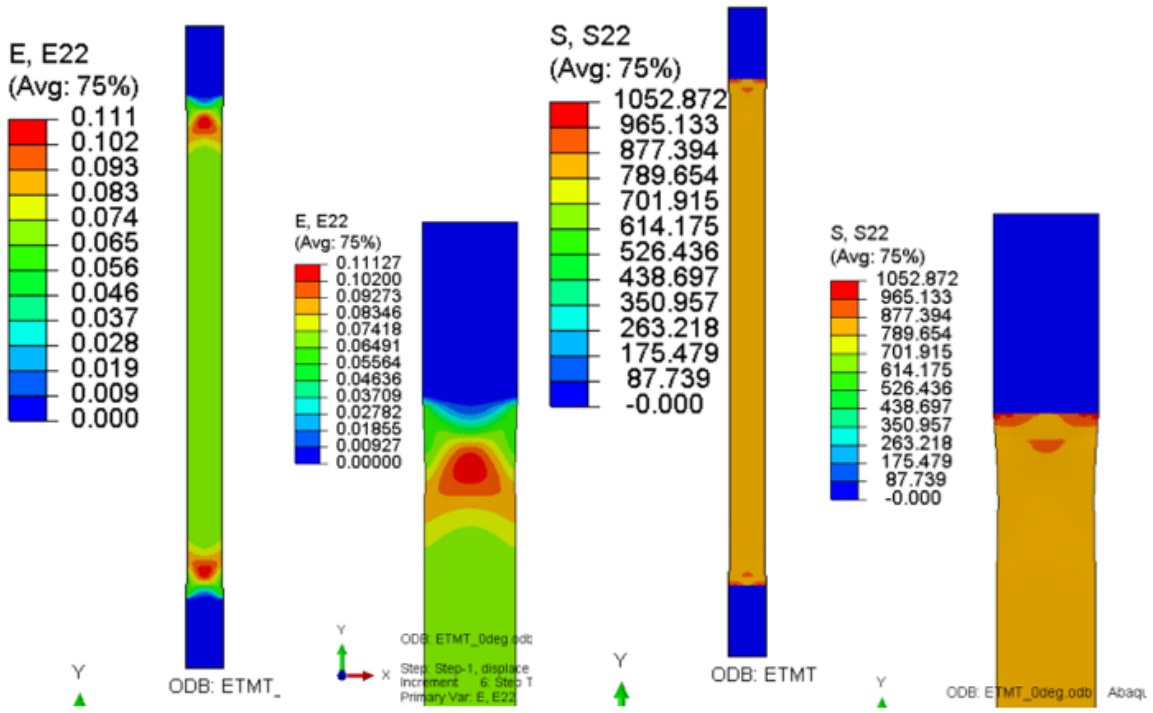

Figure 29 Strain and stress contours for an aligned straight-sided hard steel sample.

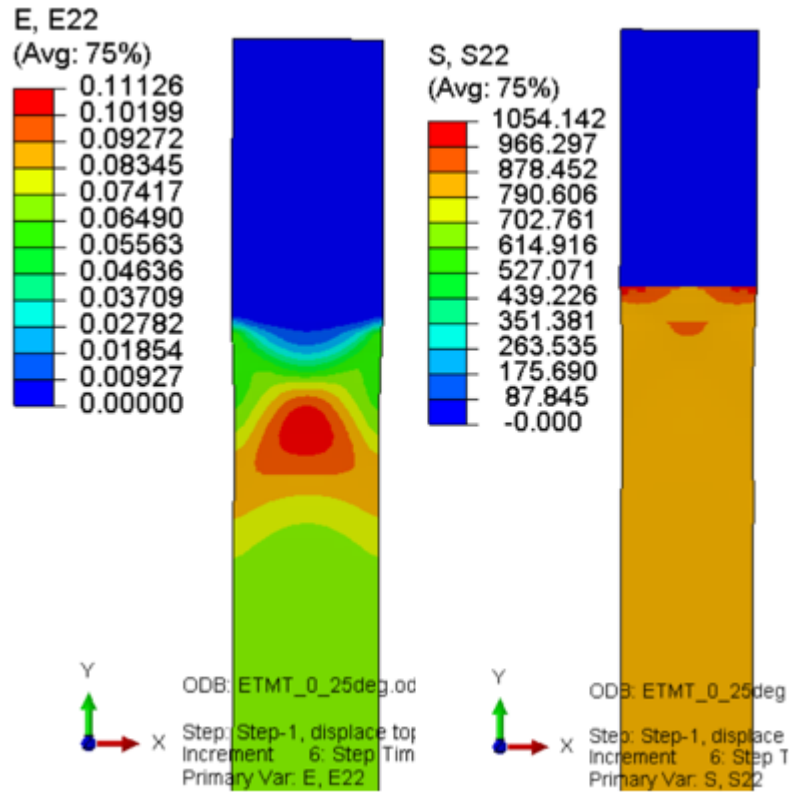

Figure 30 Strain and stress contours for a straight-sided hard steel sample offset to 0.25°.

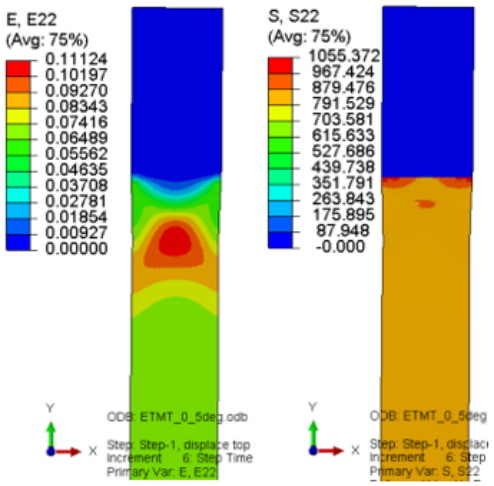

Figure 31 Strain and stress contours for a straight-sided hard steel sample offset to 0.5°.

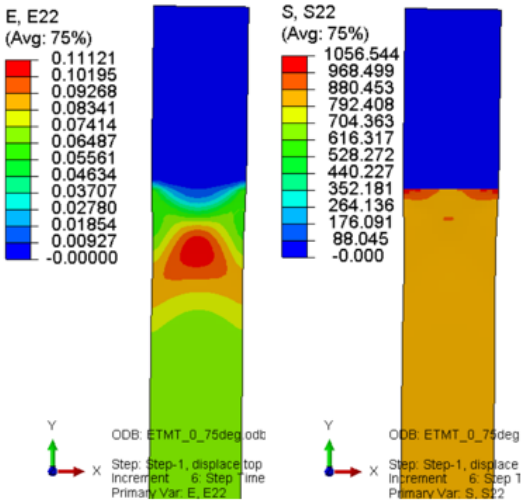

Figure 32 Strain and stress contours for a straight-sided hard steel sample offset to 0.75°.

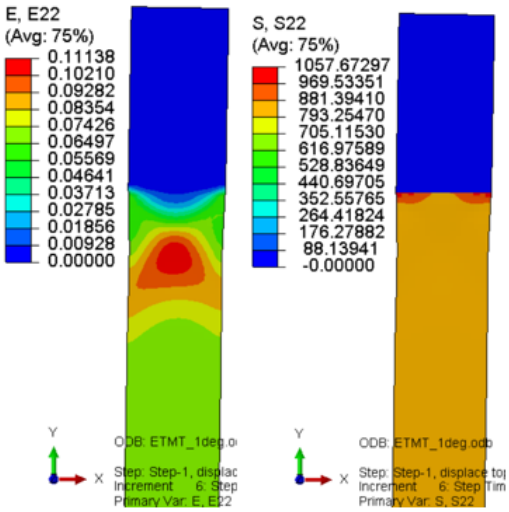

Figure 33 Strain and stress contours for a straight-sided hard steel sample offset to 1°.

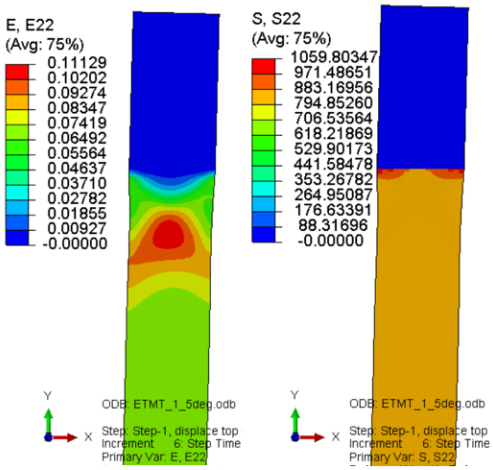

Figure 34 Strain and stress contours for a straight-sided hard steel sample offset to 1.5°.

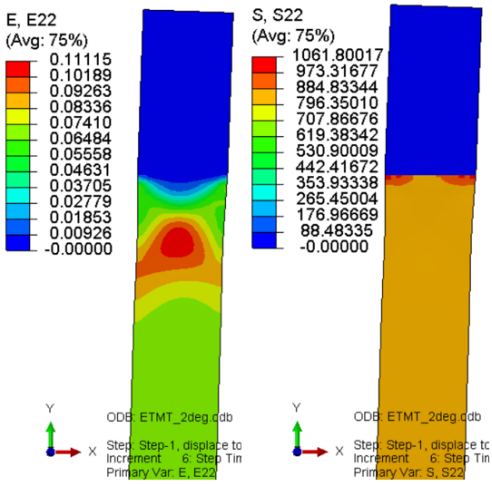

Figure 35 Strain and stress contours for a straight-sided hard steel sample offset to 2°.

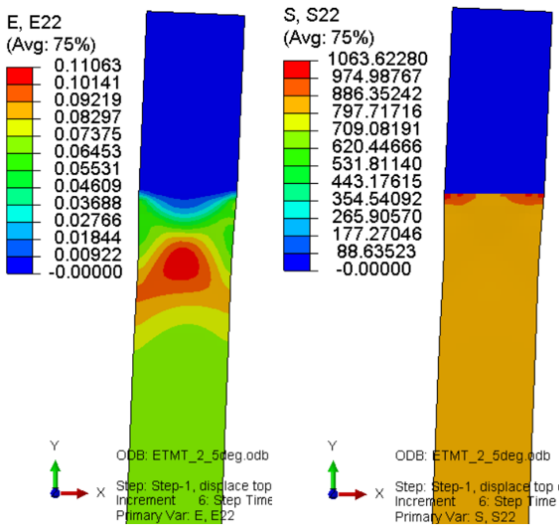

Figure 36 Strain and stress contours for a straight-sided hard steel sample offset to 2.5°.

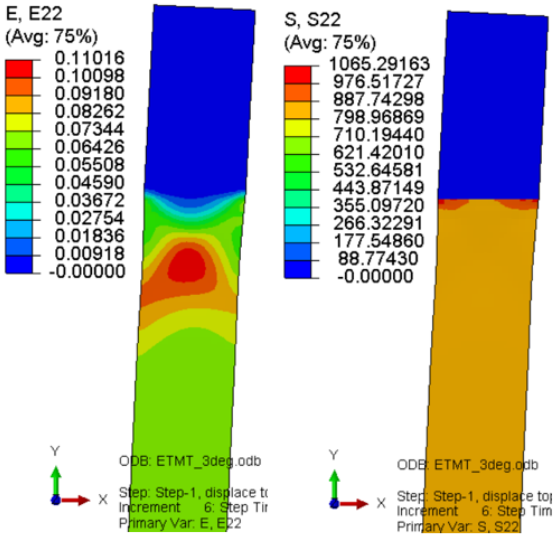

Figure 37 Strain and stress contours for a straight-sided hard steel sample offset to 3°.

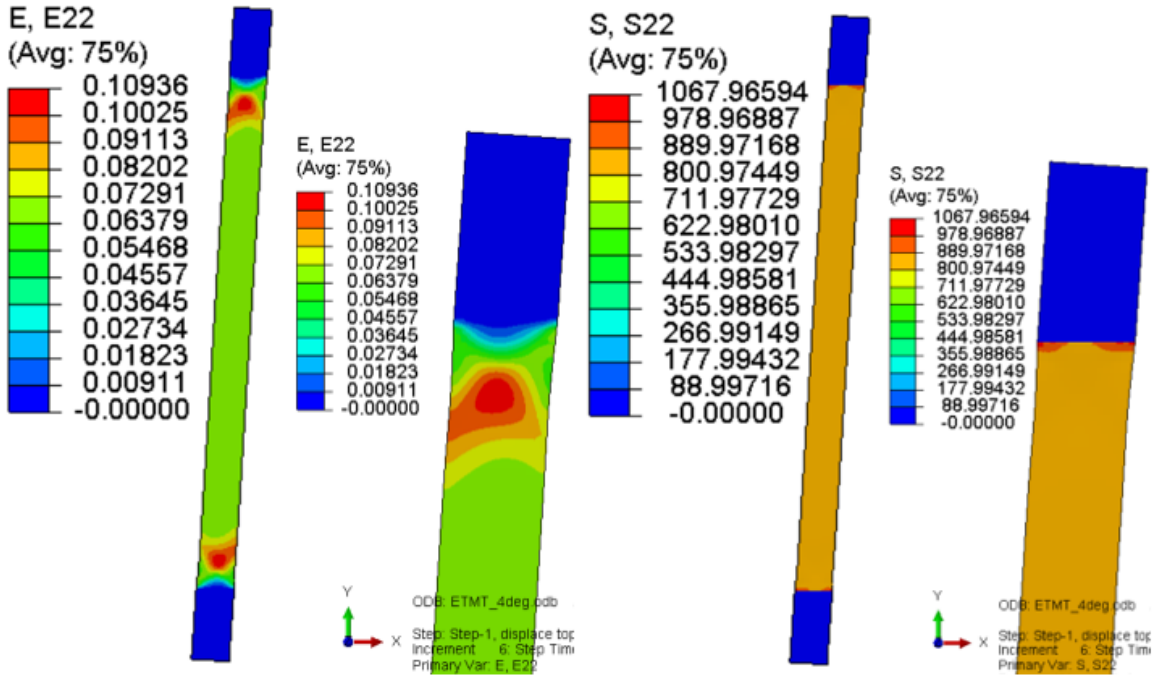

Figure 38 Strain and stress contours for a straight-sided hard steel sample offset to 4°.

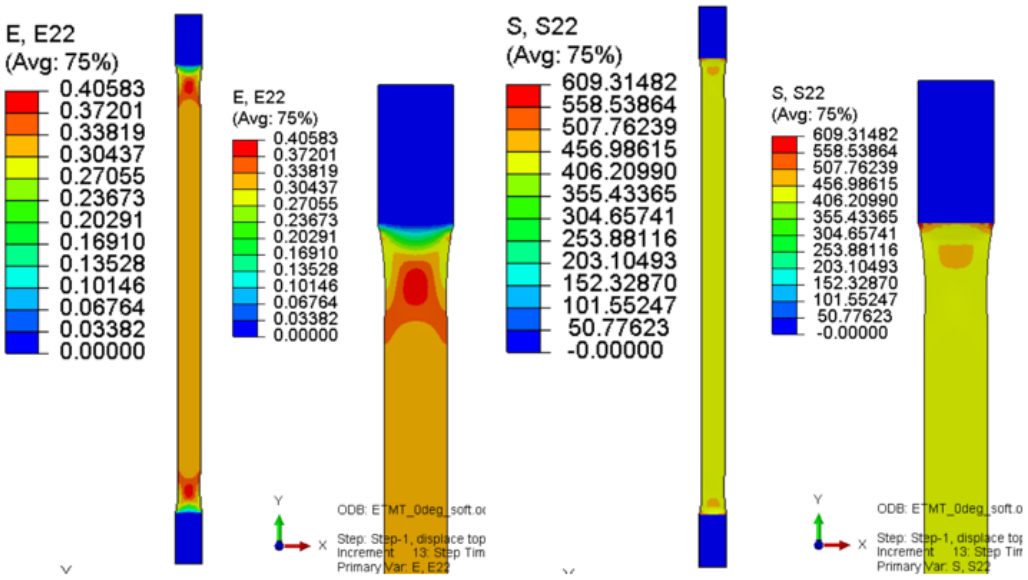

Figure 39 Strain and stress contours for an aligned straight-sided soft steel sample.

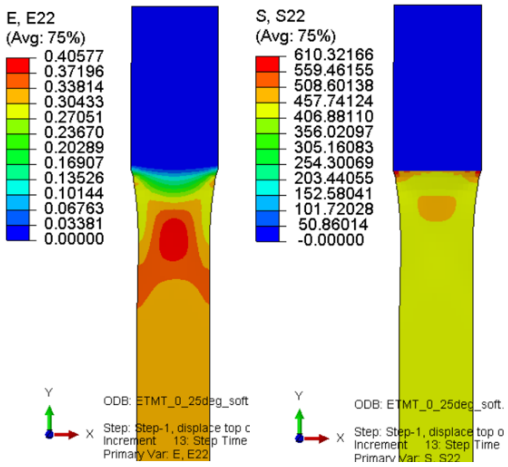

Figure 40 Strain and stress contours for a straight-sided soft steel sample offset to 0.25°.

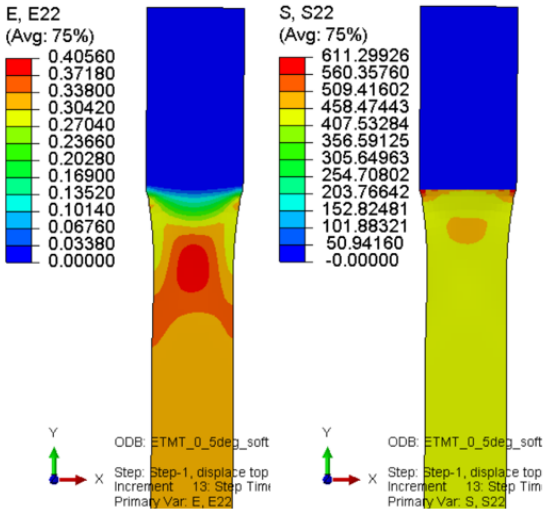

Figure 41 Strain and stress contours for a straight-sided soft steel sample offset to 0.5°.

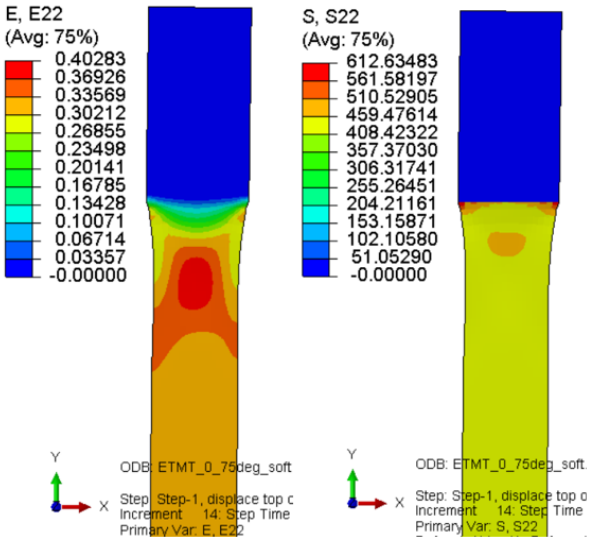

Figure 42 Strain and stress contours for a straight-sided soft steel sample offset to 0.75°.

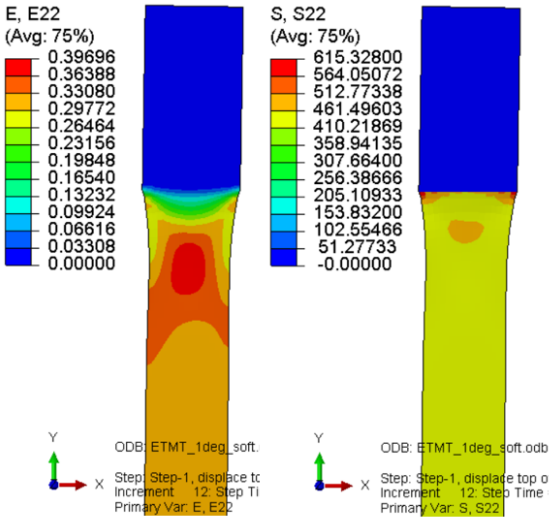

Figure 43 Strain and stress contours for a straight-sided soft steel sample offset to 1°.

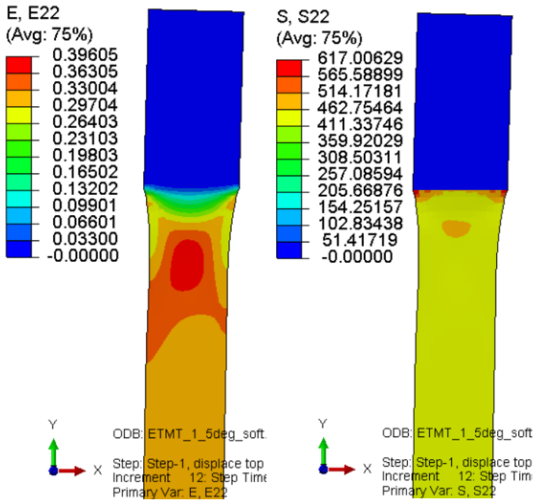

Figure 44 Strain and stress contours for a straight-sided soft steel sample offset to 1.5°.

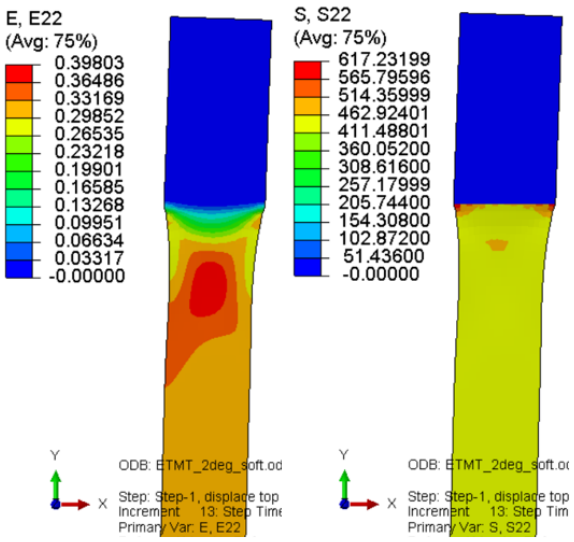

Figure 45 Strain and stress contours for a straight-sided soft steel sample offset to 2°.

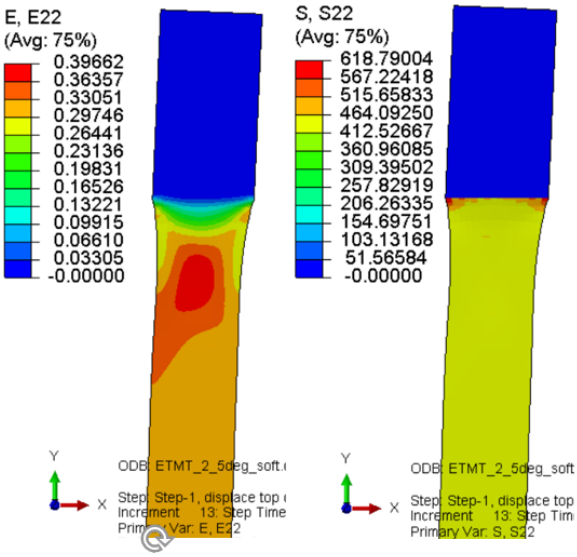

Figure 46 Strain and stress contours for a straight-sided soft steel sample offset to 2.5°.

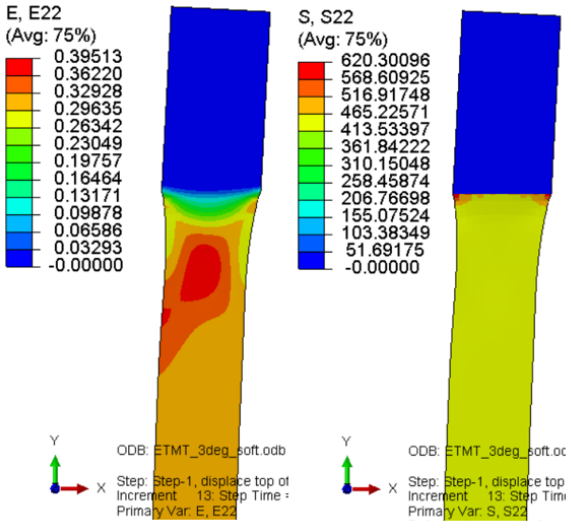

Figure 47 Strain and stress contours for a straight-sided soft steel sample offset to 3°.

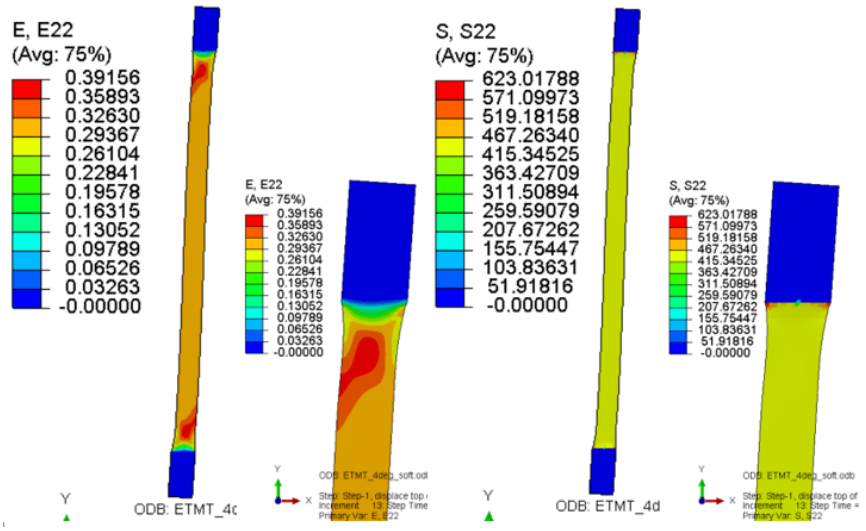

Figure 48 Strain and stress contours for a straight-sided soft steel sample offset to 4°.

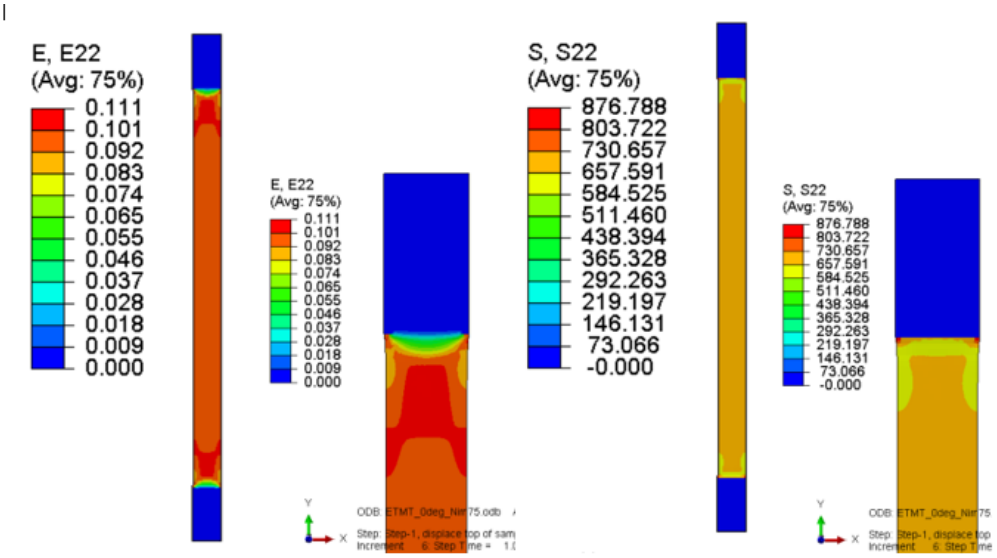

Figure 49 Strain and stress contours for an aligned straight-sided Nimonic 75 sample.

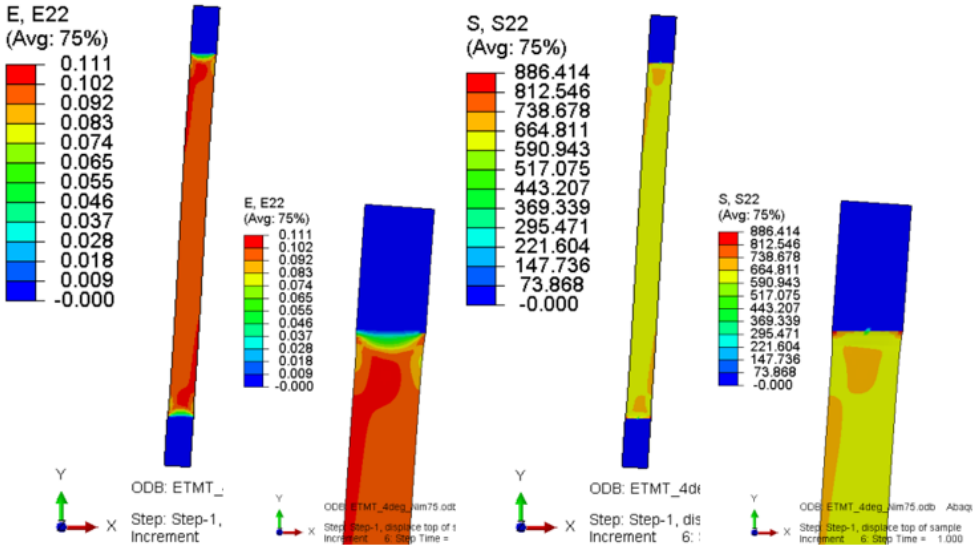

Figure 50 Strain and stress contours for a straight-sided Nimonic 75 sample offset to 4°.

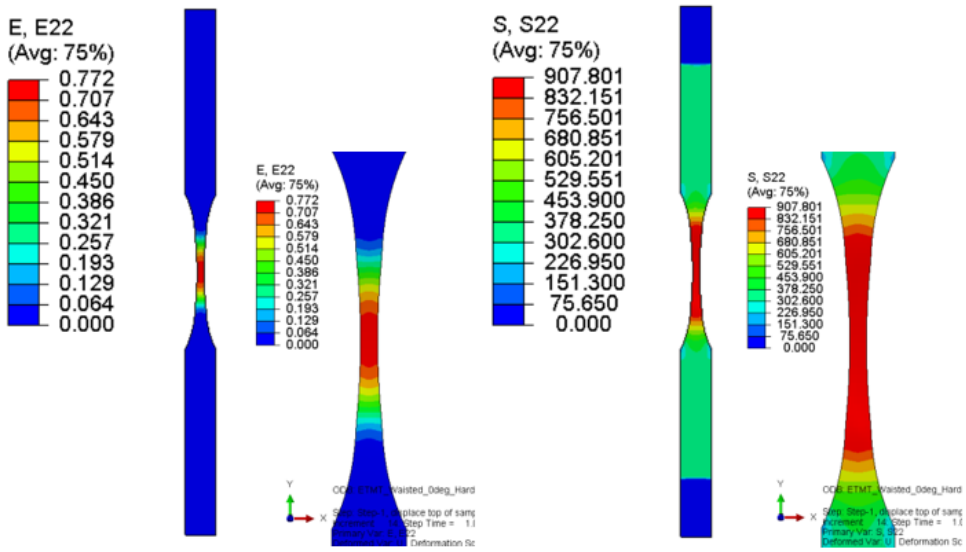

Figure 51 Strain and stress contours for an aligned waisted hard steel sample.

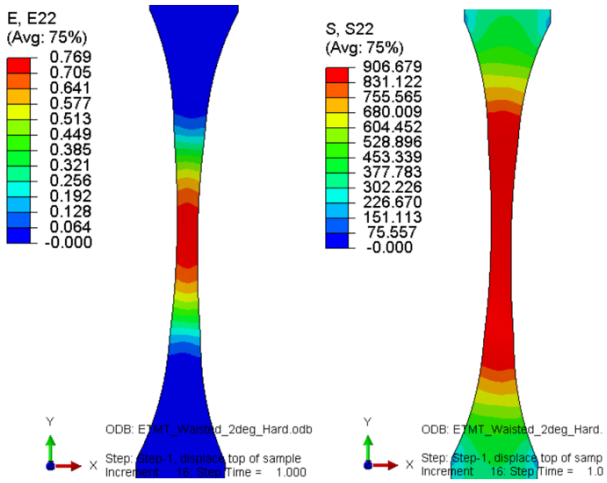

Figure 52 Strain and stress contours for a waisted hard steel sample offset to 2°.

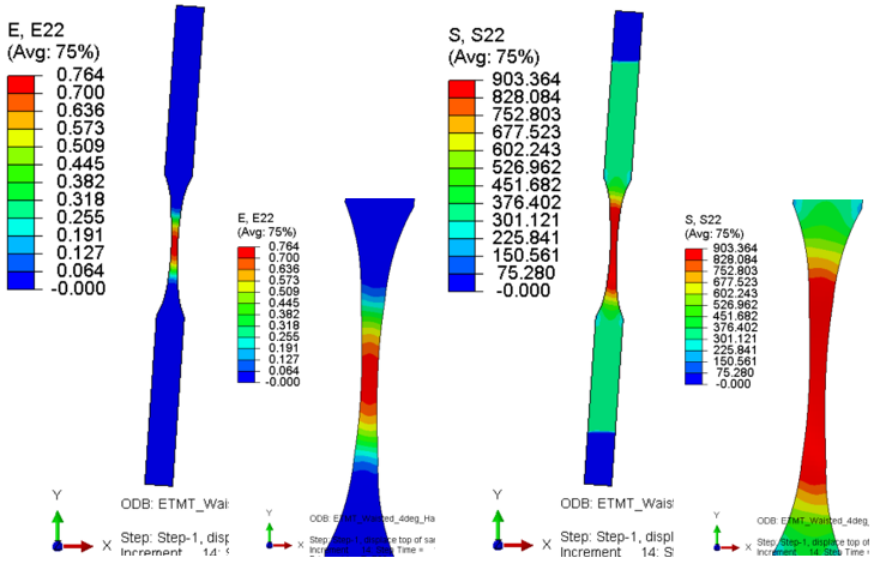

Figure 53 Strain and stress contours for a waisted hard steel sample offset to 4°.

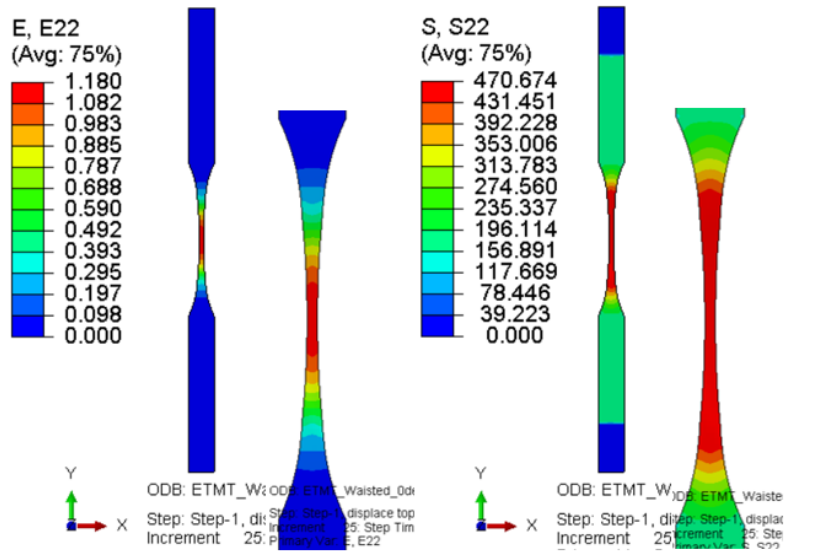

Figure 54 Strain and stress contours for an aligned waisted soft steel sample.

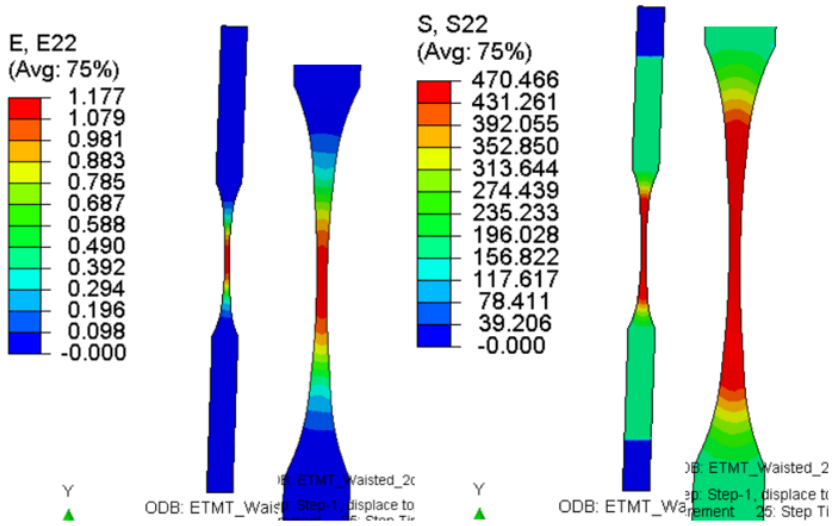

Figure 55 Strain and stress contours for a waisted soft steel sample offset to 2°.

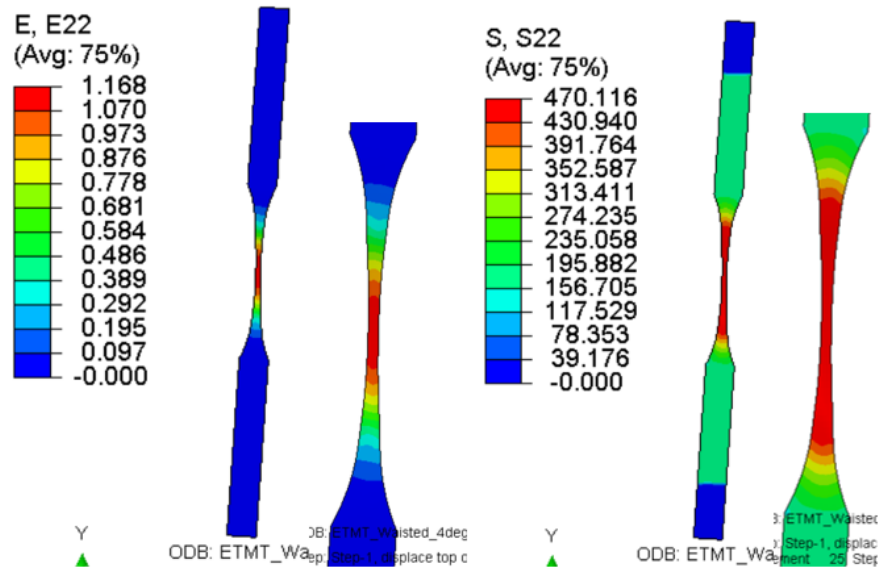

Figure 56 Strain and stress contours for a waisted soft steel sample offset to 4°.

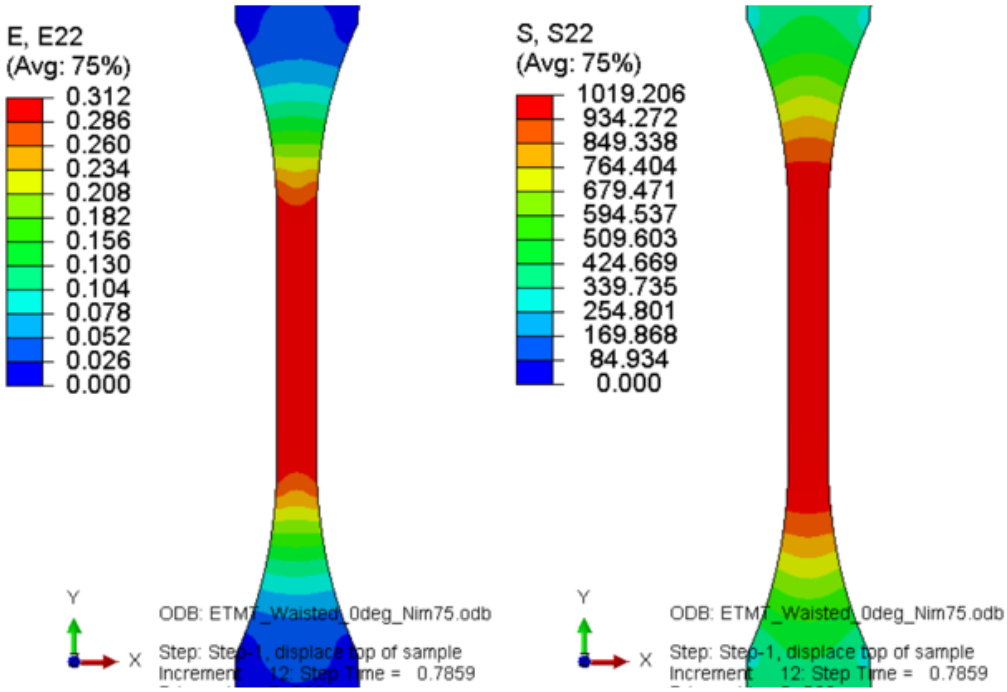

Figure 57 Strain and stress contours for an aligned waisted Nimonic 75 sample.

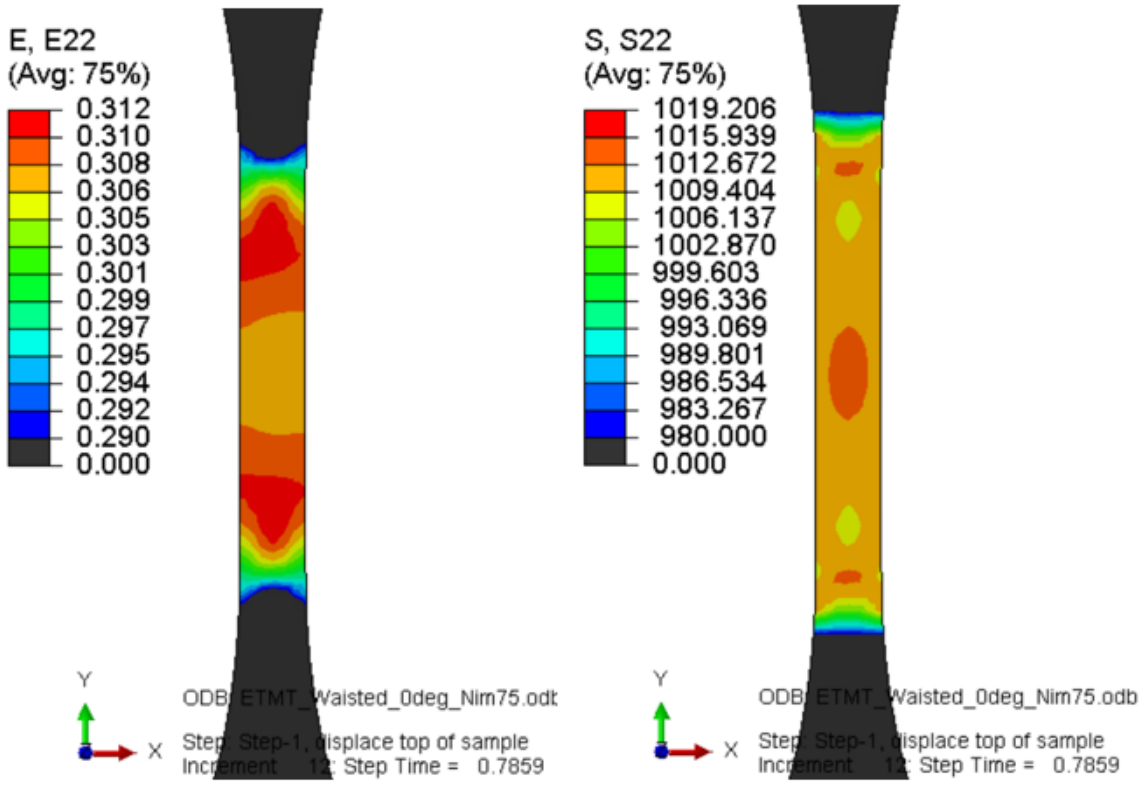

Figure 58 Strain and stress contours for an aligned waisted Nimonic 75 sample with tighter contour limits.

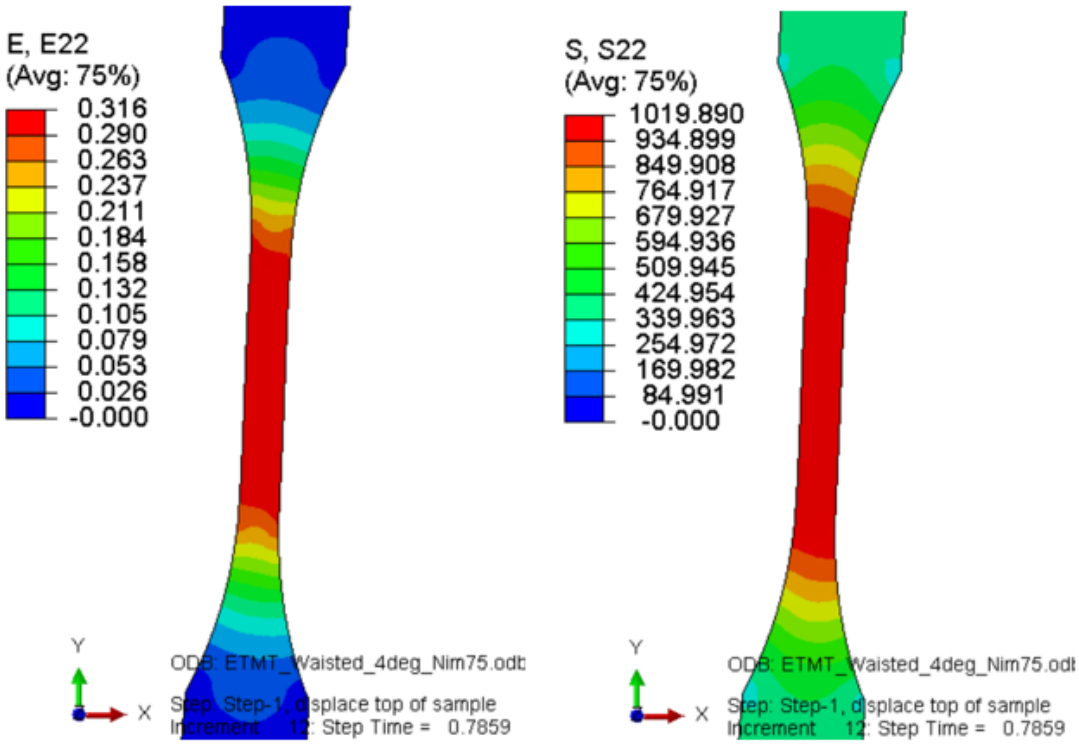

Figure 59 Strain and stress contours for a waisted Nimonic 75 sample offset to 4°.

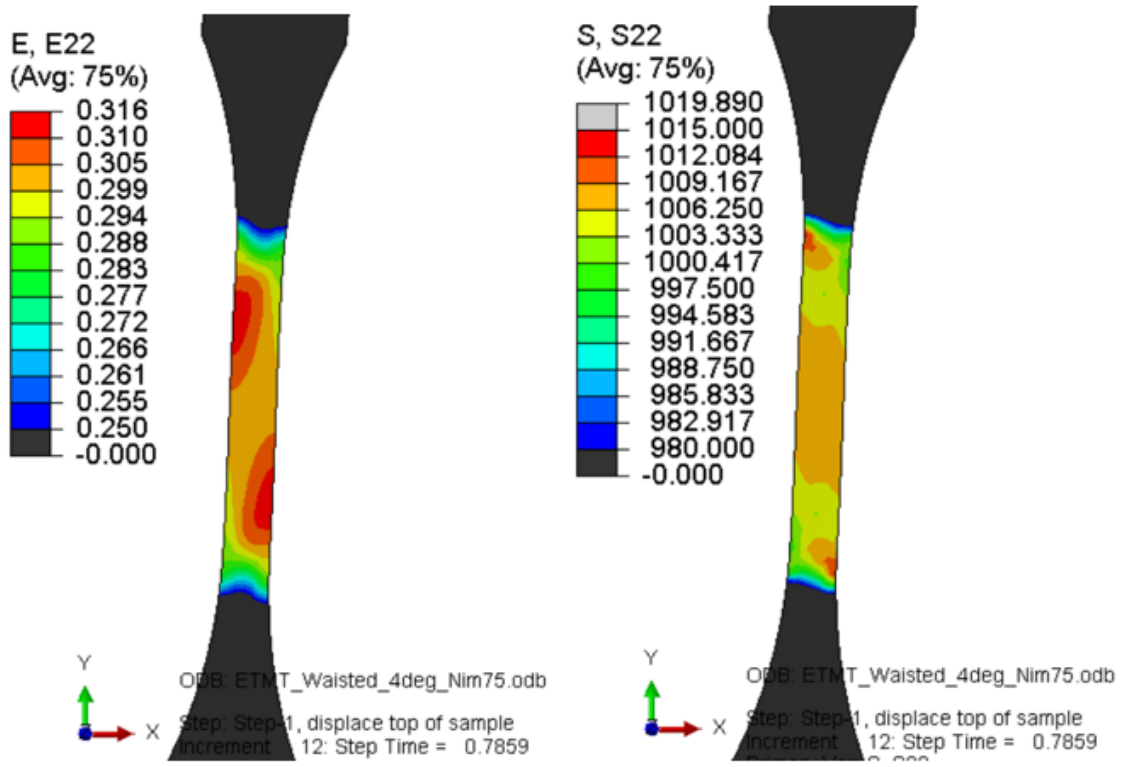

Figure 60 Strain and stress contours for a waisted Nimonic 75 sample offset to 4° with tighter contour limits.

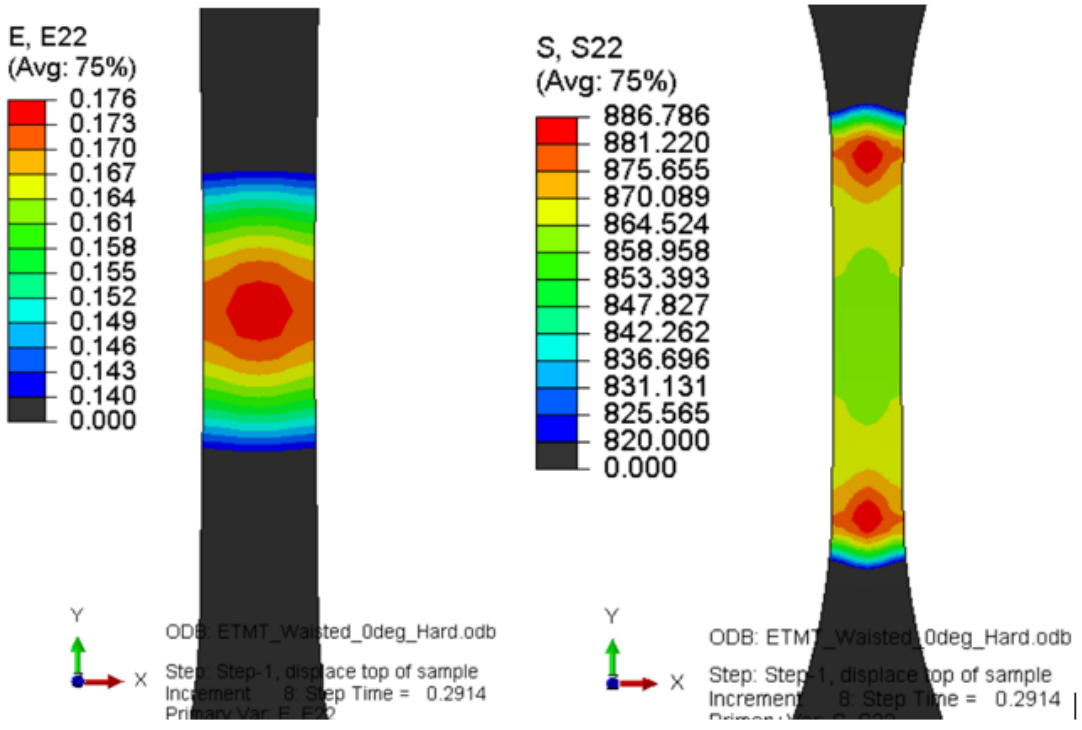

Figure 61 Strain and stress contours for an aligned waisted hard steel sample with tighter contour limits, at a displacement of 0.87 – the last point where whole central section has straight sides.

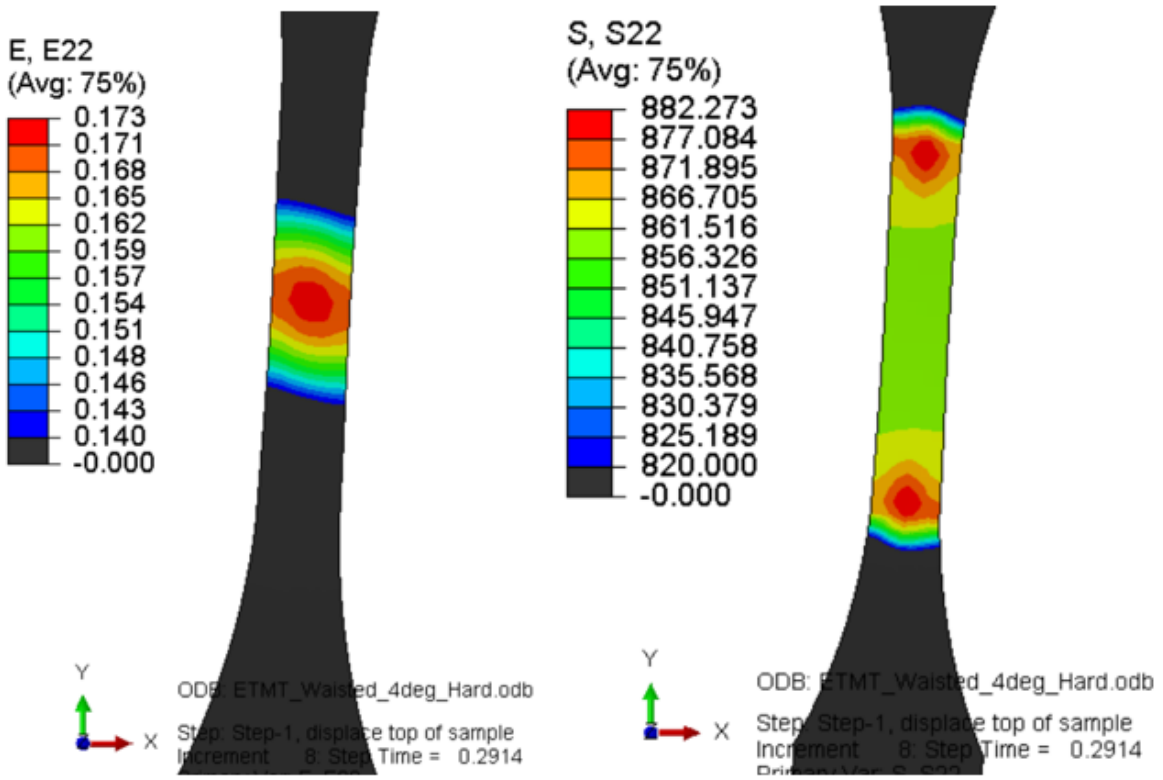

Figure 62 Strain and stress contours for a waisted hard steel sample offset to 4° with tighter contour limits, at a displacement of 0.87 – the last point where whole central section has straight sides.

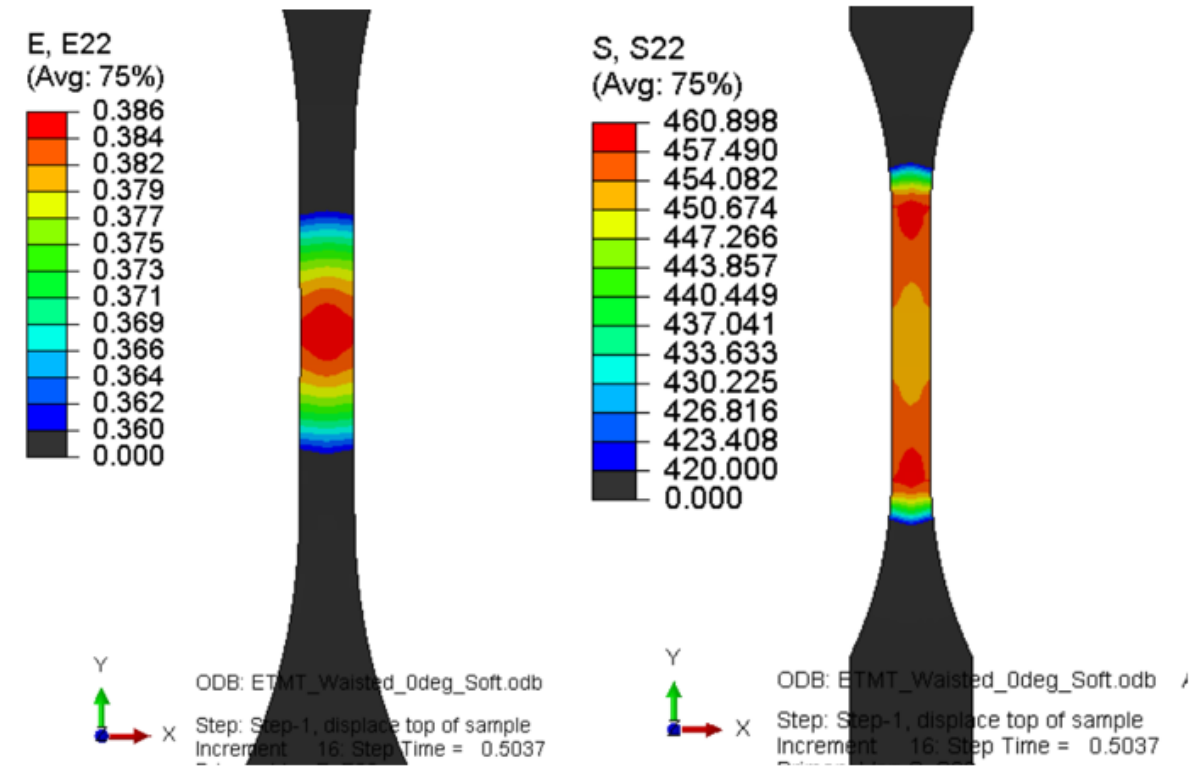

Figure 63 Strain and stress contours for an aligned waisted soft steel sample with tighter contour limits, at a displacement of 3.53 – the last point where whole central section has straight sides.

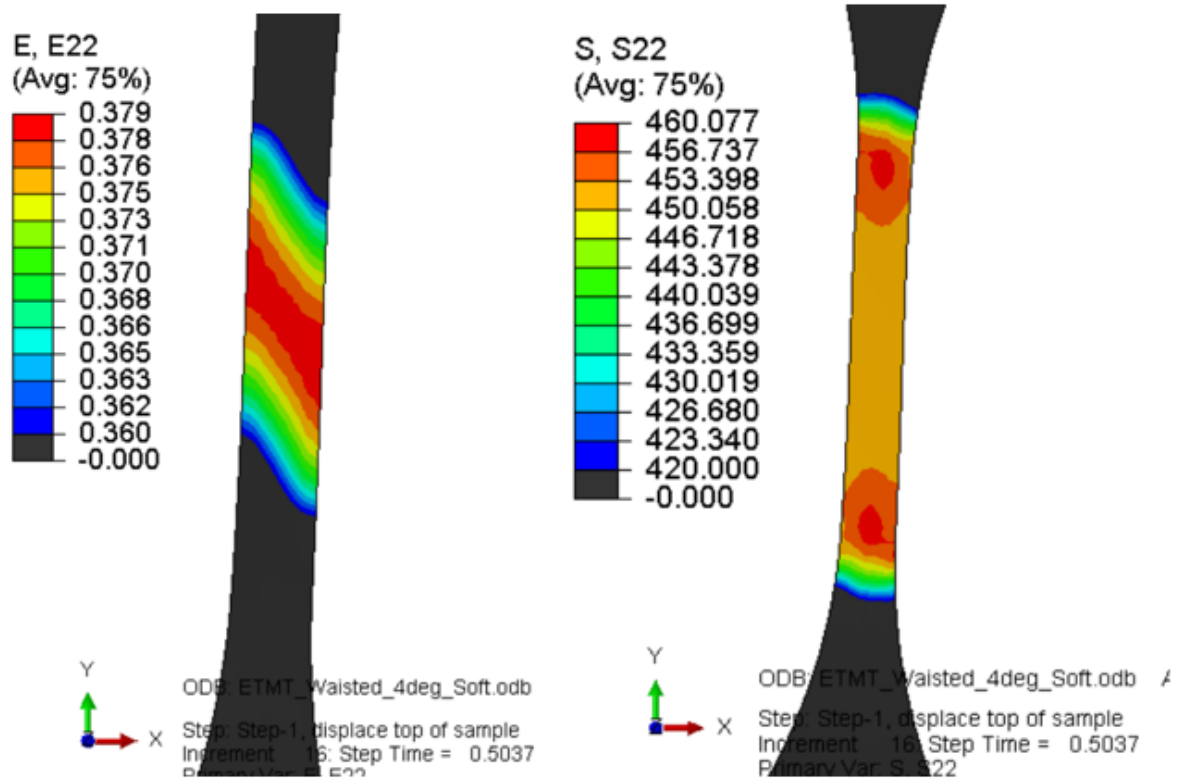

Figure 64 Strain and stress contours for a waisted soft steel sample offset to 4° with tighter contour limits, at a displacement of 3.53 – the last point where whole central section has straight sides.